Nano Today 42 (2022) 101366

Contents lists available at ScienceDirect

Nano Today

journal homepage: www.elsevier.com/locate/nanotoday

Review

Recent advances in curved image sensor arrays for bioinspired vision system

Wenchao Gao[a,b], Zhangsheng Xu[b], Xun Han[b,c,*], Caofeng Pan[b,d,*]

[a] Department of Civil Engineering, Monash University, Clayton 3800, Australia
[b] CAS Center for Excellence in Nanoscience, Beijing Key Laboratory of Micro-nano Energy and Sensor, Beijing Institute of Nanoenergy and Nanosystems, Chinese Academy of Sciences, Beijing 101400, PR China
[c] College of Mechatronics and Control Engineering, Shenzhen University, Shenzhen 518060, China
[d] School of Nanoscience and Technology, University of Chinese Academy of Sciences, Beijing 100049, PR China

ARTICLE INFO

Article history:
Received 7 October 2021
Received in revised form 18 November 2021
Accepted 28 November 2021
Available online 27 December 2021

Keywords:
Curved image sensor array
Wide field of view
Low aberration
Fabrication strategies
Artificial electronic eyes

ABSTRACT

A conventional wide-angle camera consists of a planar image sensor array and multiple optic elements, which increases the camera's volume, weight, and cost. In nature, most biological visual systems possess a curved retina, providing the capability of a wide field of view imaging with high sensitivity through a single lens. Inspired by the unique advantage of the biological eye, various curved image sensor arrays have been demonstrated, which enable a wide field of view, low aberration, and highly sensitive image acquisition with a simple lens design. Herein, various fabrication strategies for the curved image sensor arrays are summarized. In addition, the applications of the curved device in the artificial electronic eyes as well as the challenges and opportunities of the curved image sensor array are also discussed.

Contents

1. Introduction

All biological species possess the sensing capability to perceive external information from their surroundings. The eye is an essential organ of vision that can receive light information. Different kinds of

* Corresponding authors at: CAS Center for Excellence in Nanoscience, Beijing Key Laboratory of Micro-nano Energy and Sensor, Beijing Institute of Nanoenergy and Nanosystems, Chinese Academy of Sciences, Beijing 101400, PR China.
E-mail addresses: hanxun@szu.edu.cn (X. Han), cfpan@binn.cas.cn (C. Pan).

https://doi.org/10.1016/j.nantod.2021.101366
1748-0132/

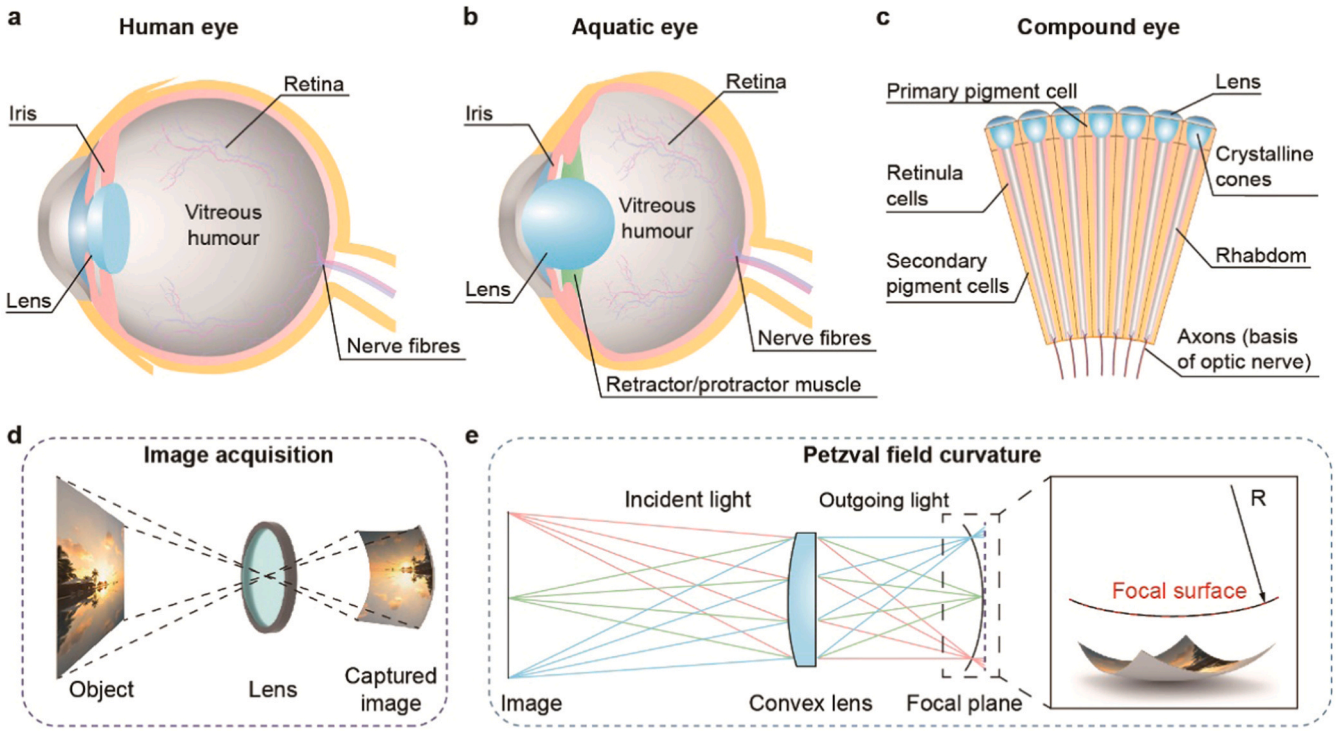

Fig. 1. Three types of biological eyes and the Petzval field curvature. Schematic illustration of the (a) human eye, (b) aquatic eye, and (c) compound eye. d, Image acquisition through a single lens showing the curved captured image. e, Schematic illustration of the Petzval field curvature demonstrating the mismatch between the curved focal plane and planar image sensor.

eyes have been found in nature with distinctive structures and functions. The simplest eyes, named ocelli, do not have the lens and can only distinguish whether the surroundings are dark or bright [1]. In contrast, the complex eye can detect the light with external information, including intensity, color, shape, and frequency [2–4]. The sophisticated and marked design of the eyes of the creatures enables unique functions with high visual acuity. For example, the color perception capability of bees allows them to find the bright flowers that contain nectar, and the highly light-sensitive eye of the fish is important for them to see the distant object in the dim underwater condition [5,6]. For the human, more functions are realized including the ability to read books, create beautiful works of art, and experience joy from the colorful nature, etc. Fig. 1a shows schematics of a human eye. It is typically roughly spherical, with a lens and iris to control the incident light intensity, filled with transparent vitreous humor and equipped with a curved retina for light detection [7]. The light with various information entered into the eye and was projected on the retina at the rear edge of the eye. And then the light was detected and converted into electrical signals, which were transmitted to the visual cortex for further image processing through the optical nerves [8]. The aquatic eyes shared a similar structure and visual process but with a fixed lens shape (Fig. 1b) [2,9,10]. Compound eyes, found in the arthropods, are composed of thousands of small photodetection units (called ommatidia), which renders a pixelated image [11–13]. Each ommatidium consists of its lens and photodetection cells, which are compactly integrated in slightly different orientations(Fig. 1c) [14,15].

All three types of the above-mentioned complex eyes demonstrate a common feature, that the retina is assembled in the hemispherical or curved format. This is because the lens's curved nature in the eyes, which projects the object in a curved manner (Fig. 1d) [16]. The curved retina, well-matched with the focal plane, provides a wide field of view (FoV) for aberration-free image acquisition with only a single lens, making the eye very compact [7]. Currently, the commercialized cameras are mainly manufactured on the planar film or wafer using the mainstream conventional fabrication process. In these optical systems, the Petzval field curvature is a common vision problem that induces image distortion in the corners of the frame (Fig. 1e) [17]. Specifically, the light traces are perfectly focused in the center of the frame and focus disappears immediately as the light traces move away from the center, resulting in a reduced resolution in the mid-frame and a much blurt image at the corners [18]. Thus, a large set of lenses is required to compensate for the field curvature and eventually eliminate the image aberration [19]. For instance, a camera with a wide FoV of 120° needs an optical lens system containing 8–13 lenses [20], which significantly increased the volume, weight, and cost of the camera. A straightforward approach to eliminate the image distortion and minimize the volume and weight of the optics is to deform the image sensor of the camera to match the curved focal plane.

Inspired by the unique advantages of the biological eyes, various curved image sensors have been proposed with wide FoV, deep depth of field (DoF), and capability of aberration-free image acquisition [21]. This review covers the recent advances of the curved image sensor array, with a focus on the fabrication strategy of the curved device and its integration with optics for the curved vision system. Five major structure designs for the construction of the curved image sensor have been discussed, which are ultrathin design, origami/kirigami, island-bridge, fractal web, and in situ growth of the nanowire, also their applications in the curved vision system have been summarized. Finally, we proposed some challenges that must be considered for further applications in smartphones, drones, and autonomous vehicles.

2. Comparison between curved and flat image sensors

Image sensor arrays shaped onto curved surfaces demonstrate additional functions inaccessible to the conventional planar devices

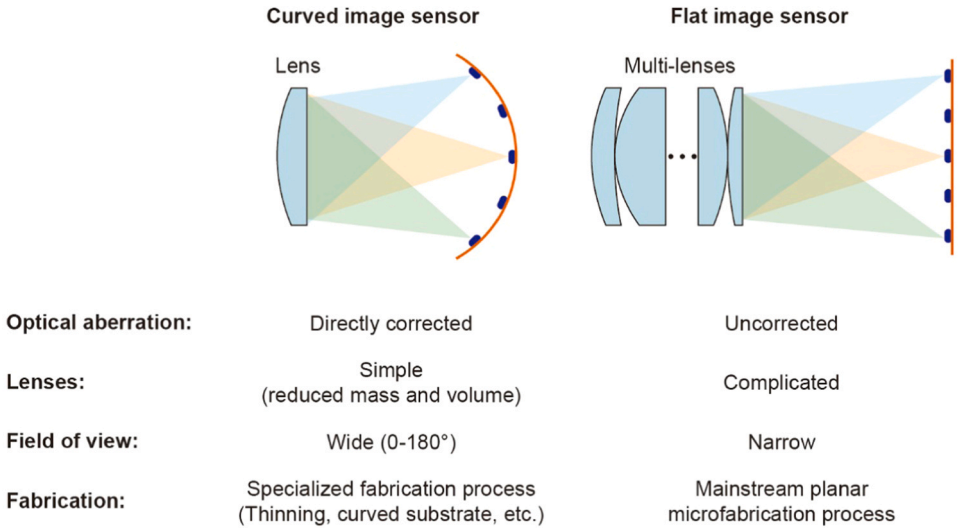

Fig. 2. Comparison between the curved image sensor and conventional flat image sensor.

[22]. By comparing the curved and flat image sensors, the differences between the two types of devices are summarized in Fig. 2. First, the curved imaging system can easily correct the optical aberration due to the small mismatch between the curved image sensor and the curved focal plane. Second, a complicated lens configuration is required in the flat image sensor to eliminate the image distortion in the corners. For example, the Double Gauss lens containing 6 pieces of the lens is used to focus an image on a planer image sensor, whereas a simple plano-convex lens could realize an object focusing on the entire curved image sensor. Thus, fewer optical elements in the curved imaging system could effectively minimize the mass/volume of the system and reduce the instrumental errors to achieve high stability. Third, the curved image sensors can offer a wide FoV for outstanding image quality even with a simple lens design. Such as, a wide FoV of 180° has been achieved in the commercialized curved complementary-metal oxide-semiconductor (CMOS) image sensor. The curvature of curved image sensors required to obtain these hardware advantages depends on the specific optical requirements. For example, in the monocentric lens design, a wide FoV could be achieved with as simple as two elements, which is commonly found in the protruding aquatic eyes. In this case, the curvature of the spherical image sensor is identical to the FoV. With the optics requirement for the curved image sensor being reduced, the barrier to realizing these advantages is to create a highly-curved image sensor with a large pixel density. Unfortunately, the CMOS world is flat. The mainstream planar microfabrication process is not compatible with the fabrication of the curved imaging system. It is challenging to achieve such large curvature as well as scale to small pixel pitches (less than 10 μm). Therefore, the innovation of the manufacturing process is expected.

3. Fabrication strategies of the curved image sensor

Curved image sensors can adapt their curvature to match with the focal plane, overcome several hardware limitations for next-generation imagers, and provide economic benefits. However, these curved image sensors are technologically challenging to fabricate. Currently, the commercialized CMOS image sensor and charge-coupled device (CCD) are mainly using the planar device architecture and manufactured by the conventional micro-/nano-fabrication processes, challenging to perform on a curved surface. Specialized fabrication strategies, including transferring, deforming, and in situ material synthesis, have been developed for curved devices. A comparison of the curved image sensor array with various fabrication strategies and device structures is summarized in Table 1.

3.1. Ultrathin design

A straightforward method to fabricate the curved image sensor array is to directly deform and press the planar device on a hemispherical surface. However, the wrinkles and folds in the device induced by bending strain will remarkably increase the mechanical failures [23–29]. This required that the planar devices to be highly flexible to survive the mechanical deformations [30–35]. A promising method is to decrease the film thickness [36–38]. The bending curvatures could be markedly enhanced by thinning the film, for example, a six order of magnitude increasing of the bending curvature can be induced by reducing the film thickness from 1 μm to 1 nm [39]. As shown in Fig. 3a, the ultrathin device could be directly pressed or laminated on the curved surface, including the concave hemispherical surface (Fig. 3b) and fingerprint (Fig. 3c) [40]. Utilizing the ultrathin structure, Thai et al. demonstrated a curved image sensor array based on the atomically thin MoS_2-graphene structure, where the bending strain induced by deformation on a hemispherical surface could in turn expand the photoresponse to the near-infrared regime [41]. Fig. 3d showed the SEM image of the photodetector array laminated on a concave hemispherical surface, where the opening diameter was 6 mm and recessed depth was 400 μm. The strain distribution on the hemispherical dome was analyzed by the FEA method (Fig. 3e). The non-uniform strain distribution was observed with the maximum strain of 1.19% located at the center of the device. Under the strain condition, the estimated bandgap demonstrated a decreasing trend with the compressive strain with a gauge factor of ~108 meV/% (Fig. 3f). The strain-induced bandgap shrinkage expands the photoresponse spectrum to the near-infrared regime. The obtained photocurrent mapping results for 0% and 1.19% strain under illumination with the wavelength from 405 to 904 nm were summarized in Fig. 3g. Compared with the unstrained device, the strained device demonstrated an enhanced photoresponsivity with a high on/off ratio under visible light illumination. More importantly, stain-induced photoresponse in the NIR range was observed under illumination at 785 and 904 nm. Due to the non-uniform strain distribution, the inner pixels under high compressive strain showed higher photoresponsivity than the outer pixels. In addition, various materials, structures and novel phenomenon have been exploited in the flexible electronics to improve the device performance [42–49]. Metal halide perovskites

Table 1
Summary of the fabrication strategies and device structures of the curved image sensor arrays. (d: diameter).

Fabrication strategy	Substrate	Pixel number	Pixel dimensions (μm×μm)	Fill factor	Structure	Wavelength (nm)	Responsivity (A/W)	Detectivity (Jones)	Response/recovery time (ms)	FoV (°)	Ref.
Ultrathin design	PI	7 × 8	~100 × 100		Graphene /MoS_2/Graphene	405, 532, 685, 785, 904	23.95		2700/3000		[41]
	Parylene-C	10 × 10	100 × 100	~11%	Au/$CsPbBr_3$/Au	450	3.15	3.94×10^{12}	8/6.5		[40]
Origami	PET	24	~320 × 305		Au/a-Ga_2O_3/Au	250	8.9	3.3×10^{13}			[69]
				~80%	Si photodiode	470, 660, 940				160	[81]
	PI		~250 × 250	~76%	MoS_2-graphene phototransistor	515, 850	2200				[82]
	PI	281	d = 113	~81%	Si photodiode	543, 594, 633	0.00949			~108	[58]
	SU-8	48	~100 × 100		MoS_2/Graphene	532	38		290/420		[68]
Kirigami	PI	32 × 32	300 × 300	~78%	Si photodiode						[79]
Island-bridge	PI	180	160 × 160	~6%	Si photodiode					160	[124]
	PI	16 × 16	~160 × 160	30%	Si photodiode	620–700			15		[97]
	PI	16 × 16	560 × 560	~33%	Si photodiode						[93]
	PI	15 × 15	d = 150	~20%	GaAs photodiode	525	0.29	1.89×10^{11}		~112	[98]
	PI	23 × 23		~10%	Si NR photodiode	850	0.34			120	[119]
Fractal web structure	PI	48	~850 × 570		PyB-doped grapheme phototransistor	440–700	> 1000		170	~90	[105]
In situ growth	AAO/PDMS	10 × 10			W/Ionic liquid/$FAPbI_3$/Eutectic GaIn		0.303	1.1×10^9	19.2/23.9	101.1	[109]

demonstrate the excellent optoelectronic properties, facile synthesis procedures and compatibility with flexible substrates, which bring the paradigm shift in the way of next-generation optoelectronic device design [50–57]. Wu et al. adopted the wafer-scale $CsPbBr_3$ perovskite film array as the active material and realized an ultrathin perovskite photodetector array with a simple 5 layers structure (Fig. 3h) [40]. The total thickness of the device is less than 2.4 μm. Benefitting from its ultrathin thickness, the device could form conformal contacts with the non-developable surface, such as the fingerprint and walnuts. A thin parylene-c film was adopted as the encapsulation layer to improve the mechanical robustness and environmental stability. As shown in Fig. 3i, the device demonstrated almost unchanged photoresponse behavior after being stored in the air for 6 weeks. Fig. 3j showed the photocurrent mapping result of the device. A clear letter of "U" can be easily recognized. The device can also capture different letters of "H" and "N", indicating its reliable imaging capability. To further minimize or avoid the folds and wrinkles in the active region induced by the bending strain, origami design and reduced pixel size can be also employed to ensure close contact with the hemispherical surface without mechanical failures [58].

3.2. Origami/kirigami design

Origami, also named paper-folding, is a facile method to directly and continuously transform a two-dimensional (2D) plane to a three-dimensional (3D) structure through folding and bending [59–63]. Versatile micro/nanoscale 3D structures have been demonstrated through the elaborately designed 2D film driven by surface tension force [64–67]. As shown in Fig. 4a, a dome-like 3D surface was achieved by simply folding the 2D film with several arms [68]. Chen et. al. manually folded a 2D film with 8 arms and deformed it onto a hemispherical surface to demonstrate a 3D solar-blind Ga_2O_3 photodetector array [69]. Due to the advantages of the 3D curved structure, the function of real-time light trajectory tracking and imaging of multipoint light spatial distribution was achieved. Combining the functional materials, system-level architecture, and delicate origami pattern design, Lee et al. presented the 3D photodetector arrays with the capability of accommodating distinctive geometries, such as hemispherical domes, octagonal prisms, and octagonal prismoids [68]. They exploited MoS_2 film as the photoresponse material and graphene as the interconnects sandwiched by two SU-8 layers. The hemispherical photodetector with 16-arm mode reduces the maximum strain to 2.17%, which is lower than the 6% tensile limit of graphene [70–73]. Imaging capabilities encompassing the detection of incident light direction and angular divergence were demonstrated.

In contrast, kirigami, also named paper-cutting, usually consists of both the "cutting" and "folding" process. In many studies, the pre-patterning procedures were not counted, thus, there is no clear boundary between origami and kirigami. In addition, some kirigami designs could enable a sort of stretchability of the planar object if it can endure bending and twisting stress [74–77]. For example, Blee et al. applied the kirigami design to graphene film and achieved the stretchable graphene in the solution with excellent mechanical properties [78]. As shown in Fig. 4b, a stretchable planar 2D film was constructed through exquisite cutting pattern design. The film can be transferred to the hemispherical surface and form conformal contact with the curved surface due to its 30% maximum biaxial stretchability [79].

The abovementioned arm design in the Ga_2O_3 and MoS_2 photodetectors requires a large separation distance between pixels for electrical interconnects and limit the resolution of the image sensor array [80]. The truncated icosahedron, combining several pentagonal and hexagonal faces, can be recognized as a quasi-spherical solid in geometry mathematics. This geometry is typically found in the

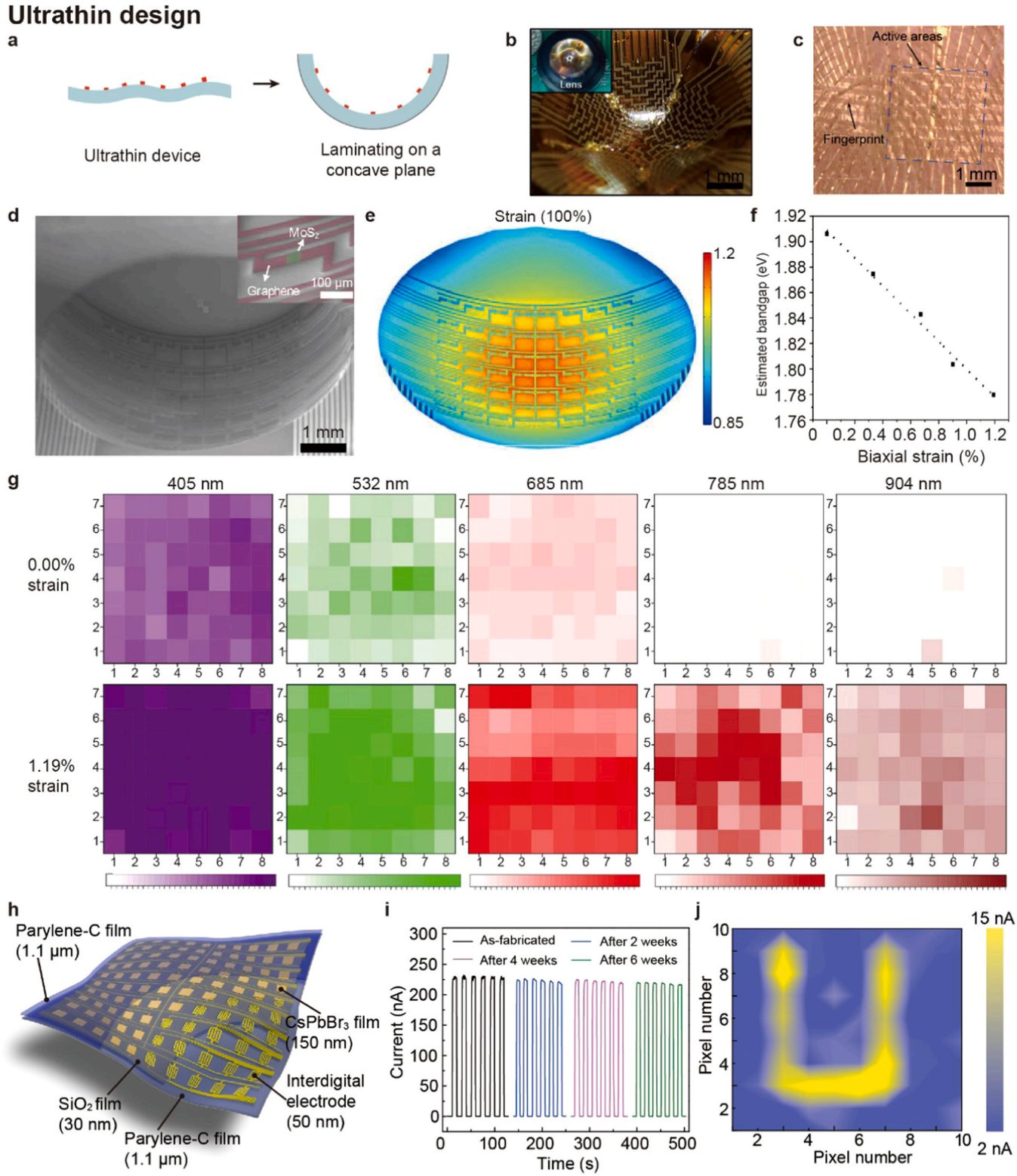

Fig. 3. Ultrathin curved image sensor array. a, Schematic illustration of an ultrathin device laminated on a concave plane. Optical image of the ultrathin device forming conformal contact with (b) a concave plane and (c) the fingerprint. b, Reproduced with permission [58]. Copyright 2017, Nature Publishing Group. d, SEM image of a MoS_2/Graphene photodetector pressed on a hemispherical concave mold. The magnified SEM image shows a single pixel laminated on the curved surface. e, Strain distribution of the curved device simulated through FEA. f, Bandgap changes induced by the biaxial strain. g, Enhanced photoresponse of the device by the biaxial strain under the illumination with the different light wavelengths of 405, 532, 685, 785, 904 nm. d-g, Reproduced with permission [41]. Copyright 2021, American Chemical Society. h, Schematic illustration of the structure of the $CsPbBr_3$ ultrathin photodetector array. i, I-T curves of the ultrathin device after fabricated and stored in the air for 2, 4, and 6 weeks. j, A U-shaped image captured by the ultrathin device. c, h-j, Reproduced with permission [97]. Copyright 2021, Wiley-VCH.

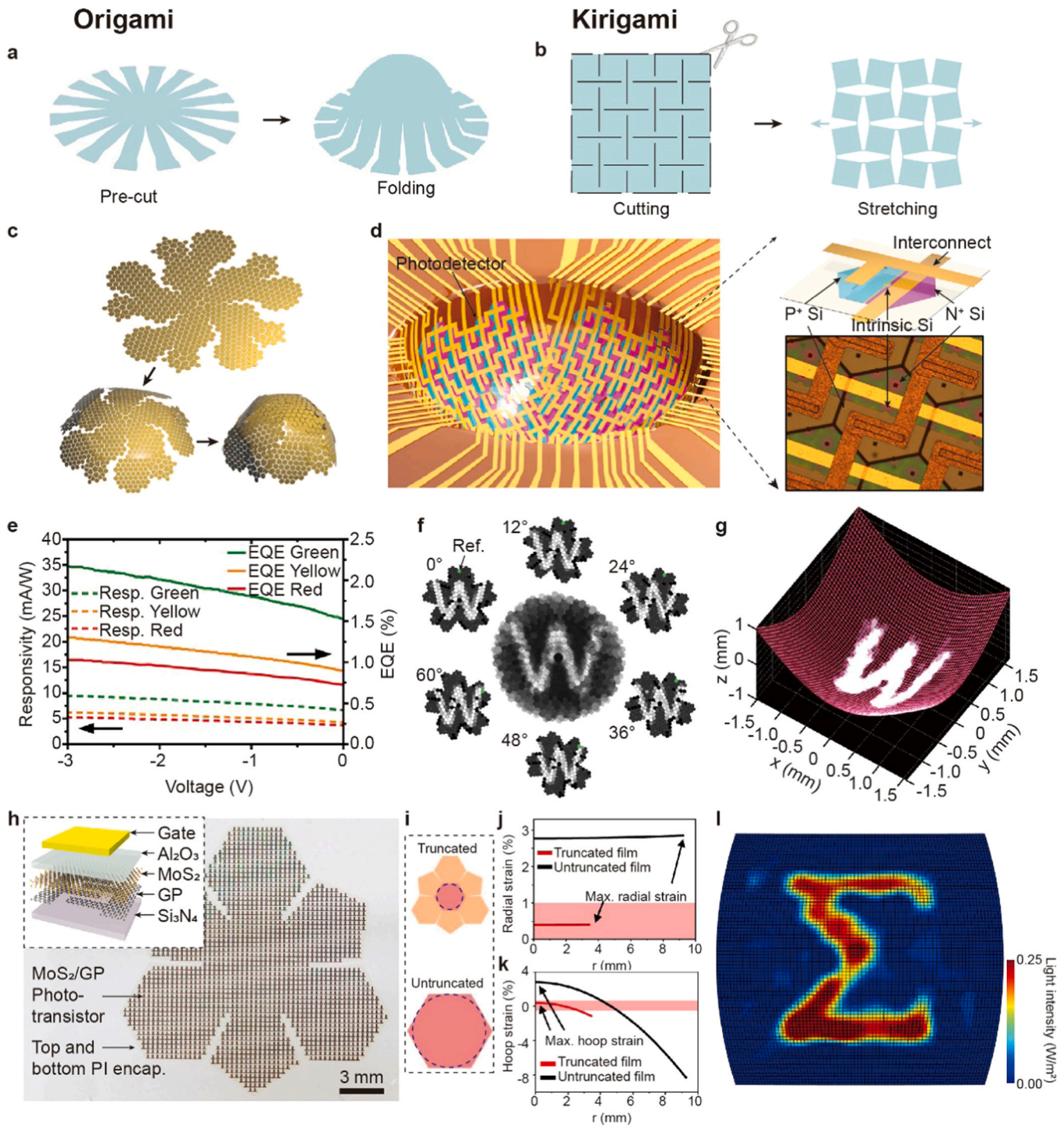

Fig. 4. Origami/kirigami design enabled curved image sensor array. a, Schematic illustration of the folding process of an origami-designed film for a 3D hemisphere. b, Schematics showing the stretchability endowed by the kirigami design. c, Schematic illustration of a truncated icosahedron-designed film being folded into a hemisphere. d, Schematics showing a Si photodiode array with truncated icosahedron design laminated on a concave mold to form a hemispherical geometry (left panel) and the device structure of a single pixel (right panel). e, Responsivity and EQE of a Si photodiode as a function of bias voltage under green, yellow and red illumination. f, A W-shaped imaged captured by the Si photodiode array with refinement by scanning every 12°. g, The capture image matching with the hemispherical geometry. c-g, Reproduced with permission [82]. Copyright 2017, Nature Publishing Group. h, Optical image of a MoS_2/graphene phototransistor array with the truncated design. Inset shows the structure of a phototransistor. i, Schematic illustration of the truncated and untruncated film for strain analysis. Radial (j) and hoop (k) strain as a function of the radius of the two films. l, A sigma-shaped image acquired by the curved MoS_2/graphene phototransistor array. a-e, Reproduced with permission [109]. Copyright 2017, Nature Publishing Group. (For interpretation of the references to colour in this figure legend, the reader is referred to the web version of this article.)

soccer balls and C60 molecules. Wu et al. employed the spring-connected silicon hexagons to achieved high fill factor of 80% [81]. Zhang et al. presented a high-density Si photodiode focal plane array using the truncated icosahedron design with each polygon block as an individual pixel [58]. Fig. 4c demonstrated a planar film folding process consisting of 676 polygon blocks for a hemispherical half truncated icosahedron, showing the transformation mechanism of this curved focal plane array. As shown in Fig. 4d, each pixel contained a Si-based lateral p-i-n junction with a wide photoresponse spectrum and fast response, and it was integrated by metal

interconnects forming a hemispherical surface. The capability of photo-sensing of a single Si photodiode was measured and plotted in Fig. 4e. Under the green, yellow and red illumination, the device demonstrated stable photoresponse with the maximum responsivity and external quantum efficiency (EQE) of 9.49 mA/W and 2.2%, respectively. Fig. 4f and g demonstrated the imaging capability by a curved camera which assembled the curved Si focal plane array and a plano-convex lens. The curved camera acquired a clear image of the letter "W". To further improve the image quality, the curved camera was rotated 60° with a step of 12° in the counterclockwise direction to take 6 photos that were combined and reconstructed (Fig. 4f). Fig. 4g presented a high-resolution image after reconstruction to match the hemispherical surface. The resolution is expected to be enhanced by minimizing the scan steps. Imaging was performed under green light illumination due to the large photoresponse to the green light.

To improve the mechanical stability of the curved device, Choi et al. reported a high-resolution and hemispherical curved image sensor based on the similar truncated icosahedron design but using MoS_2-graphene heterostructure as the active material (Fig. 4h) [82]. The use of inherently soft material, strain isolation design, and truncated icosahedron architecture enables close contact with the hemispherical surface and decreases the possibility of mechanical fractures [83–87]. Theoretical analyses of the strain distribution were performed to corroborate the validity of the truncated design. Fig. 4i demonstrated the simplified models that the truncated pattern was recognized as a small circular film surrounded by 6 separated polygon blocks, while the untruncated design was approximated as a large circular film. As shown in Fig. 4j and k, the tensile strain in the truncated film was significantly reduced compared with the untruncated design. Both the maximum radial and hoop strains are less than 1%, ensuring the integrity of the material after deforming to a hemispherical surface [88]. The curved MoS_2-graphene sensor also demonstrated the capability to capture various images. An alphabet sigma was successfully visualized by the device (Fig. 4l). It's worth noting that the imaging process will not be affected by the IR light, due to the relatively large bandgap of MoS_2 film, whereas IR noises always appear in the conventional Si image sensors.

3.3. Island-bridge structure

Island-bridge structure can also be employed to construct a stretchable system of rigid materials to enable curved shape transformation [89–92]. As shown in Fig. 5a, the rigid "islands" are fixed on the planar pre-stretched substrate and the "bridges" usually adopt the metal wire/line interconnects with serpentine shape to increase the mechanical robustness [93,94]. During releasing of the substrate, compressive force drives the substrate to return to its original shape and moveable "bridges" deform to a new layout without electrical and mechanical failure [95,96]. The stretchability of this structure is determined by the substrate pre-stretching process and deformity of these "bridges". Fig. 5b demonstrated a 16 × 16 photodetector array transferred and laminated on a hemispherical surface. The arc-shaped interconnect enabled the transformation from planar to hemispherical with the capability of shape accommodation and reproducible deformation (Fig. 5c). By using the island-bridge structure, Jung et al. demonstrated a hemispherical focal plane array based on the Si photodiode with adjustable zoom capability, where the rigid Si film was separated by the serpentine metal trace and transfer printed on an elastomer substrate [97]. Driven by the water pressure substrate, the device with the elastomer deformed and stretched into a hemispherical shape with tunable curvature (Fig. 5d). The change of the serpentine metal trace geometry accommodated the entire layout's transformation without mechanical fracture. The finite element analysis (FEA) of the strain distribution of a 2 × 2-unit cell was presented in Fig. 5e. The calculated maximum strain under the overall biaxial stretch of 12% was far below the fracture strain of the Si photodiodes and metal interconnects. A fluidic lens with a tunable shape was integrated with the curved Si focal plane array to demonstrate the zoom function. As shown in Fig. 5f, four images with different optical magnifications from 0.24 to 0.83 were collected through tune the lens shape and the curvature of the Si focal plane array. The magnification of the image was 3.5 and the uniformity of the images was obtained for all four configurations. It is obvious that the pixel density changed after transferring the island-bridge device onto the curved surface. To make sure the pixel spacing is constant after transferring, Fan et al. demonstrated a general strategy for the transformation of the planar device into a strain-free 3D structure by exploiting the shear-lip motion on the PDMS surface [98]. A hemispherical image sensor array was proposed using this strategy without loss of array resolution, which demonstrated its potential application in fabrication of the high-density curved sensor array.

3.4. Fractal web structure

The spider webs in nature that possess the repeating pattern offer the excellent capability to resist various mechanical stress from the environment [99–102]. Inspired by the spider web, the fractal web design even with few cuts of the spiral threads combines the properties of connecting strength and web stretchability with strain uniformly distribution in the entire web [103,104]. As shown in Fig. 6a, a fractal web that mimics a planar spider web could adapt its shape to integrate with the hemispherical surface without an obvious mechanical mismatch. Through assembling the optoelectrical materials/devices on the web, Lee et al. demonstrated a 3D photodetector array on a hemispherical dome (Fig. 6b) [105]. They positioned the photodetector pixels on the junction of the spiral and radial threads, which were connected by the Au serpentine traces along the radial threads (Fig. 6c). As shown in Fig. 6d, the transistor architecture was adopted for photodetection with the PyB doped graphene served as the active material. The fractal designs allowed the device to be seamlessly laminated on a hemispherical dome. The device could be repeatably attached and detached from the dome with various diameters due to its good mechanical robustness. Fig. 6e showed the imaging result of a laser beam which have a polar angle of 45° between the z-axis and x-y plane. The accuracy of the position detection of the laser beam could be further enhanced by decreasing the spot size and improving the device resolution.

3.5. In situ growth of nanowires

The above-mentioned manufacturing strategies of the curved image sensors are based on two fundamental processes of device fabrication on the planar surface followed by transferring onto the curved surface, which will inevitably introduce external stress into the device after transferring or even result in yield loss [106–108]. To synthesize the photoresponse materials directly in a hemispherical template could avoid the damage of the device during the transfer process, as shown in Fig. 7a. Gu et al. developed a vapor phase deposition method to grow the single-crystalline $FAPbI_3$ perovskite nanowires inside a hemispherical porous aluminum oxide membrane (PAM) (Fig. 7b) [109]. The nanowire arrays demonstrated a pitch of 500 nm, representing a high density of 4.6×10^8 cm^{-2}. Designing the proper electrical contact for the high-density nanowire arrays, they proposed a spherical biomimetic electrochemical eye. Fig. 7c demonstrated its detailed structure. The perovskite nanowires functionalized as the active materials and the tungsten film on the aluminum hemispherical shell served as the counter electrode. Between the aluminum shell and PAM template, the ionic liquid was filled in the cavity and contacted with the tungsten electrode and perovskite nanowires, mimicking the vitreous humor of the human eye. The flexible liquid metal wires were connected with the perovskite wire for signal collection and

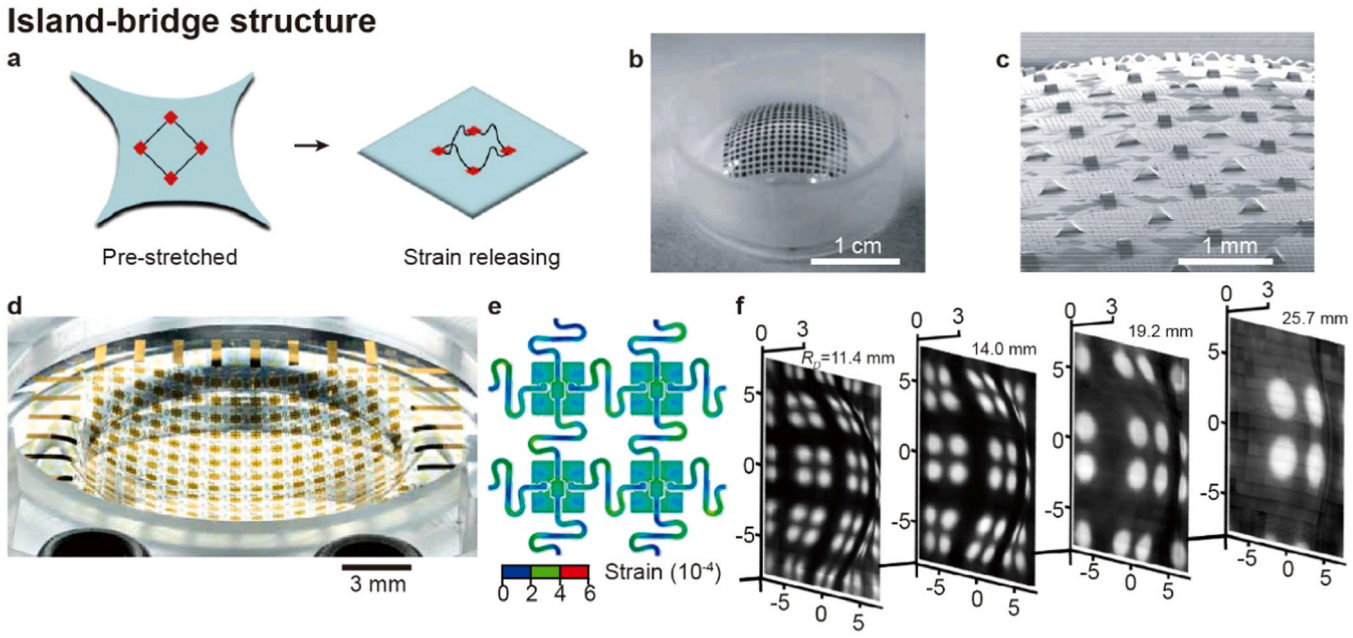

Fig. 5. Curved image sensor with island-bridge structure. a, Schematic illustration of the island-bridge structure on a pre-stretched substrate. b, Optical image of a compressed Si photodetector array on a curved PDMS surface. c, SEM image of the Si photodetector array showing the compressed interconnects. b-c, Reproduced with permission [93]. Copyright 2008, Nature Publishing Group. d, Optical image of the Si photodiode array on a thin PDMS film in the hemispherically curved condition. e, Strain distribution of the device under a 12% biaxial stretch simulated through FEA. f, Images captured by the Si photodiode array at various conditions. The radius of curvature of the device surface was tuned to match with different lens setup conditions. d-f, Reproduced with permission [97]. Copyright 2011, National Academy of Sciences.

transmission, which also determined the pixel number and density of the device. Fig. 7d showed the optical image of the integrated electrochemical eye. The incident light was absorbed under the external illumination, and electron-hole pairs were generated and separated inside the perovskite nanowires. As shown in Fig. 7e, the electrons transported to the interface between ionic liquid and perovskite and combined with the ions inside the ionic liquid to participate in the redox reactions of I^-/I_3^- pairs to contribute to the photoresponse [110]. Fig. 7f demonstrated the asymmetric I-V characteristics under different illumination intensities, indicating the different carrier transport mechanisms at the two ends of perovskite nanowires. The response and recovery time depend on the kinetics of redox reactions at the interface, and they could be further improved by increasing the concentration of ionic liquid. The dependence of the responsivity and

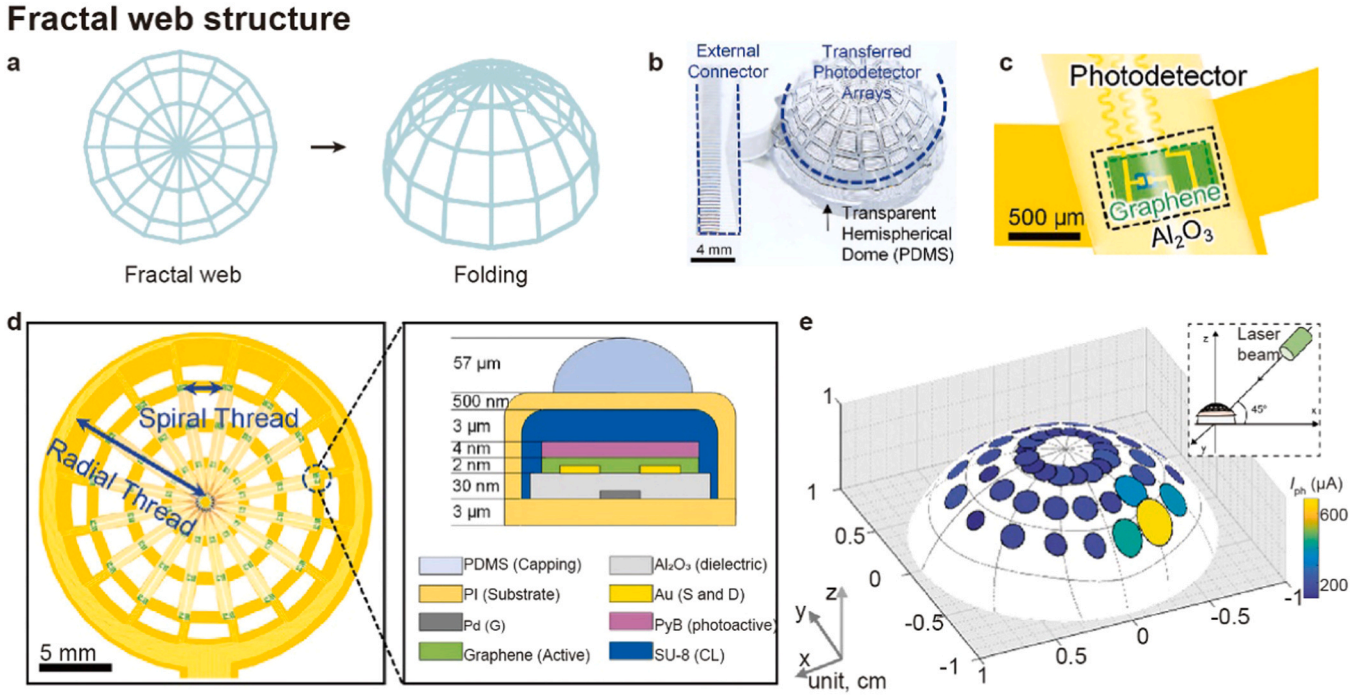

Fig. 6. Curved image sensor with fractal web structure. a, Schematics showing the folding process of a fractal web. b, Optical image of the PyB-doped graphene photodetector array laminated on a hemispherical PDMS dome. c, Enlarged view of a single pixel and Au serpentine interconnects. d, Schematic illustration of pixel distribution on the fractal web substrate. Inset shows the device structure of a single pixel. e, Photocurrent mapping results by focusing the laser beam on the device. b-e, Reproduced with permission [105]. Copyright 2020, Wiley-VCH.

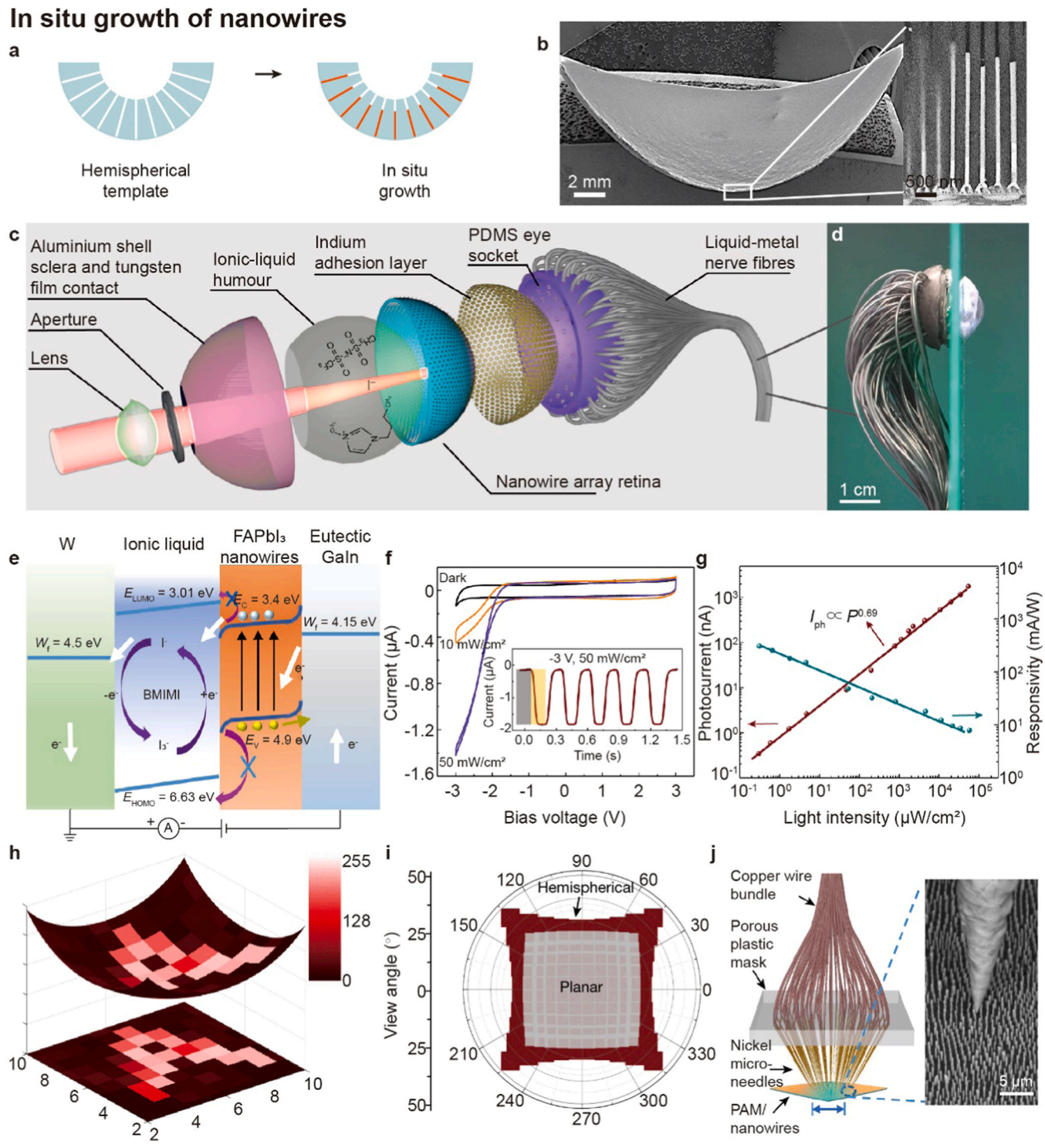

Fig. 7. Spherical electrochemical eye based on the in situ growth of perovskite nanowires inside the hemispherical template. a, Schematics showing the in situ growth process of $FAPbBr_3$ nanowires in a hemispherical template. b, SEM image of the hemispherical PAM template/nanowires and its cross-sectional SEM image. Detailed structure (c) and optical image (d) of the spherical electrochemical eye. e, Band diagram of the spherical electrochemical eye showing the working mechanism under external voltage. f, I-V curves of a single pixel under different illumination intensity and transient photoresponse under the illumination of simulated sunlight (inset). g, Photocurrent and responsivity of a single pixel as a function of illumination intensity. h, An A-shaped image captured by the spherical electrochemical eye and its projection on a flat plane. i, Comparison of the FoV between curved and flat sensors. j, Schematics showing the strategy to improve the resolution by using the Ni microneedle to contact with the nanowires array. Reproduced with permission [109]. Copyright 2020, Nature Publishing Group.

photocurrent on the illumination intensity was illustrated in Fig. 7g. The photocurrent increased linearly with the intensity, while the responsivity demonstrated a decreased trend. The maximum responsivity of 303.2 mA/W was achieved at a small intensity of 0.3 μW/cm^2. A programmed light with the shape of the letter "A" was utilized to characterize the imaging capability. 100 liquid metal wires were connected with a 100 × 1 multiplexer to collect the electrical signals. The electrochemical eye captured a clear "A" shaped image and no crosstalk was observed due to the physical separation of each pixel by the liquid metal wires (Fig. 7h). In addition, the hemispherical

electrochemical eye demonstrated a wide visual field of 100.1°, whereas that of the planar device was about 69.8° (Fig. 7i). To further improve the spatial resolution of the electrochemical eye, a novel contact strategy by using the nickel micro-needles to replace the thick liquid metal fiber has been proposed, as shown in Fig. 7j. Each needle was contacted with three nanowires, unprecedently reducing a lateral pixel size to 1 μm and pitch to 200 μm.

4. Curved vision system with visual accommodation

Biological eyes are an important vision organ with sophisticated and marked design. Numerous devices have been investigated inspired by the materials, structures, and functions of biological eyes, such as the anti-reflective coatings, electronic frog eyes, and radiant heaters [111–114]. The camera, a revolutionary invention inspired by the eye, has been unprecedentedly improved on image resolution, DoF, and intelligent functions with the software approach. Biomimicry using curved image sensors combined with a single lens will further extend the camera's functionalities, including the low aberration, wide FoV, and infinite DoF.

4.1. Human eye-inspired curved imaging system

The human eyes can see both the near and far objects by tuning the lens's shape [115,116]. In the curved imaging system, the curvature of the image sensor array is required to be changeable to accommodate the shape of the lens to minimize optical aberration [117]. Rao et al. demonstrated a shape-adaptive curved imaging system based on a 32 × 32 Si photodiode array [79]. Fig. 8a showed the schematic diagram of the curved imaging system, which consisted of a plano-convex lens with a curved image sensor on its focal plane. As shown in Fig. 8b, the kirigami design was adopted to provide the image sensor with stretchability. The device exhibited excellent mechanical robustness with no electrical failure under the biaxial strain of 30%. Additionally, the kirigami design offers a superior fill factor of 78% of the device before stretching. The device structure of a single-pixel was demonstrated in Fig. 8c. Each pixel consisted of two lateral diodes (a photodiode and a blocking diode) based on the Si p-i-n junction which is connected in a back-to-back manner to eliminate the crosstalk between pixels. The doping and isolation process was performed on a silicon-on-isolator wafer followed by a transfer-printing step to the PI substrate and metallization to connect the individual pixels. The imaging system

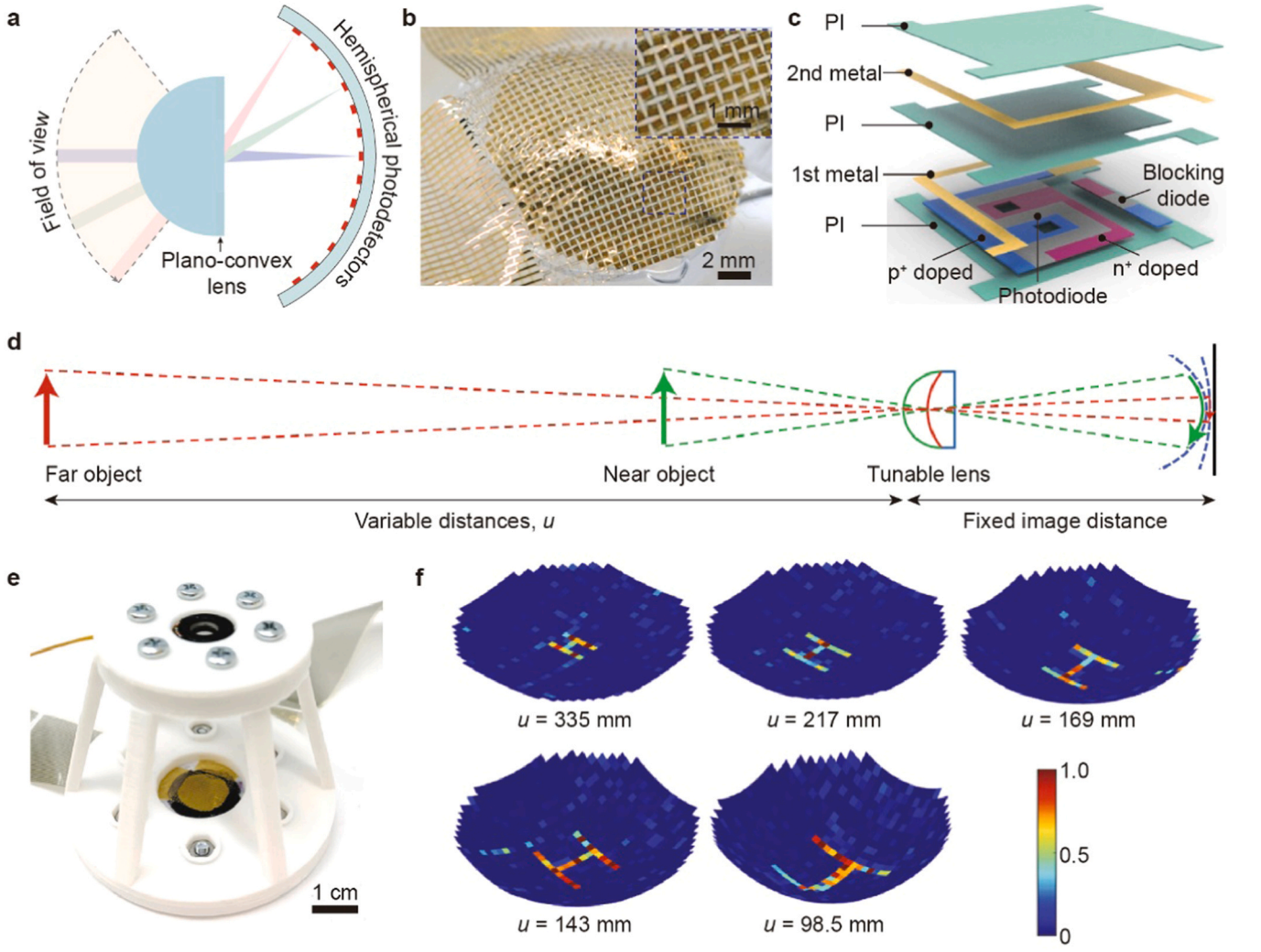

Fig. 8. Human eye-inspired curved imaging system. a, Schematic illustration of the human eye-inspired camera with a plano-convex lens and a hemispherical photodetector. b, Optical image of a Si photodiode array with kirigami design laminated on a hemispherical convex surface. c, Schematics showing the device structure of a Si photodiode pixel. d, Schematic illustration of the visual accommodation process of the curved image sensor to see far and near objects. e, Optical image of the adaptive camera integrated with the curved Si photodiode array device and a tunable lens. f, Images captured by the adaptive camera for objects at various distances. Reproduced with permission [79]. Copyright 2021, Nature Publishing Group.

was built by integrating the curved Si image sensor and a shape-adaptive lens. The curvature of the lens was tuned to be large to see the near object and became small for the far object (Fig. 8d). Fig. 8e shows the assembled curved imaging system. To demonstrate its capability of visual accommodation, such as the low aberration imaging and tunable optical focus, the image distance was fixed, whereas the object was positioned from far to near. When the object moved close to the lens, the curvature of both lens and curved image sensor increased. The imaging result of the object at different distances is summarized in Fig. 8f, showing a series of well-focused images with small optical aberration.

4.2. Aquatic vision-inspired curved imaging system

Aquatic eyes, mainly consisting of a spherical protruding monocentric lens where the refractive index (RI) is distributed in a parabolic shape along the diameter and a hemispherical curved retina, are featured in a wide FoV up to 160°, low optical aberration, deep DoF. Different from dynamically tunable lens shape structure in the human eyes, the visual accommodation of aquatic eyes is achieved by moving the lens back and forth [118]. And the highly sensitive photoreceptor on the retina ensures a clear view in the dim underwater condition. Inspired by the aquatic eyes, Kim et al. demonstrated an artificial imaging system by assembling a hemispherical Si nanorod photodiode retina (h-SiNR-PDA) and a monocentric lens (Fig. 9a) [119]. Mimicking the spherical lens in the aquatic eyes, the monocentric lens was designed with sphere and symmetric shape, where the half-ball lens with small RI and shell lens with large RI were assembled on both sides of the aperture (Fig. 9b). The customized RI of the outer shell and inner lens enables a small focal spot size while mimicking the parabolic RI profile. Due to the hemispherical retina was matched with the curved focal plane of the monocentric lens, the light incident from wide-angle can

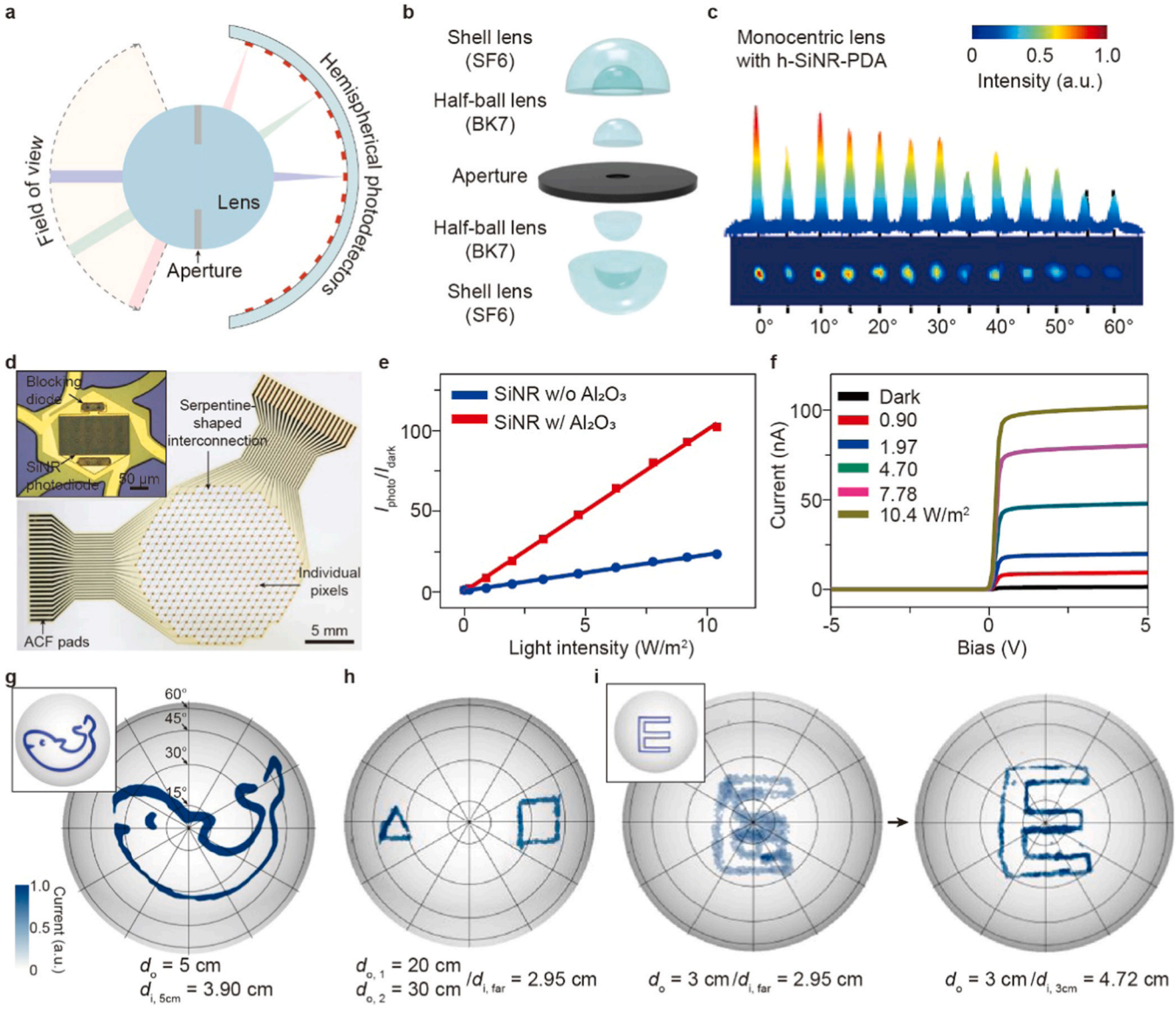

Fig. 9. Aquatic vision-inspired curved imaging system. a, Schematic illustration of the fish eye inspired camera with a monocentric lens and a hemispherical photodetector. b, Detailed structure of the customized monocentric lens. c, The light intensity and spot size at different incident angles from 0° to 60° detected through the monocentric lens and SiNR photodiode array. d, Optical image of the SiNR photodiode array on a planar surface. Inset shows a single pixel consisted of a photodiode and a blocking diode. e, On-off ratio of a single pixel with and without Al_2O_3 passivation under different light intensities. f, I-V curves of a single pixel under different light intensities. g, Image captured by the device with FoV of 120°. Inset shows the original object. h, Images acquired by the device of two objects located at different distances and different angles. i, Visual accommodation process of the device. Inset shows the original object. Reproduced with permission [119]. Copyright 2020, Nature Publishing Group.

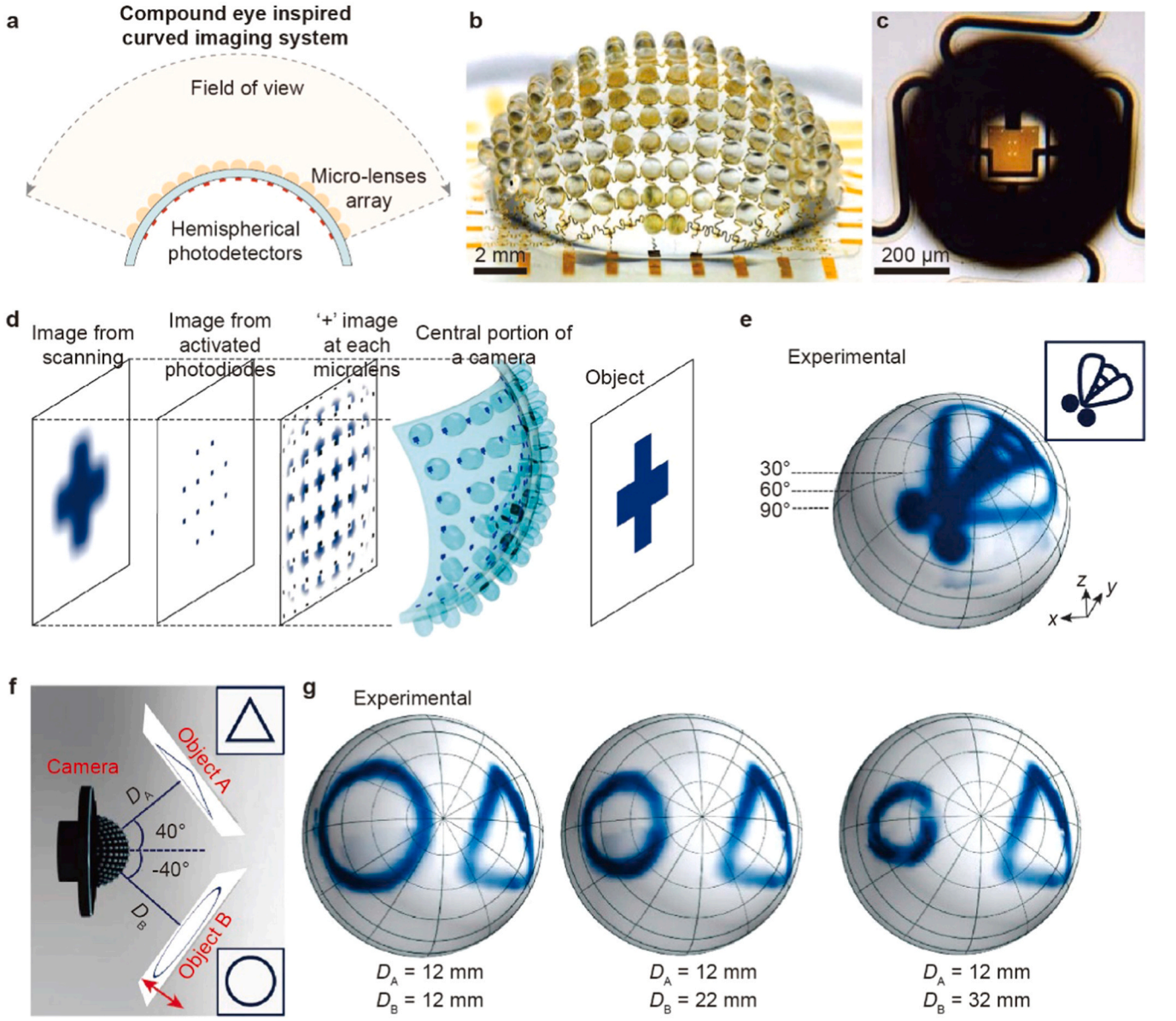

Fig. 10. Arthropod eye-inspired curved imaging system. a, Schematic illustration of the compound eye type camera with a micro-lens array and a hemispherical photodetector. Optical image of (b) the compound eye type camera and (c) an ommatidium. d, Mechanism of the image formation of the compound eye type camera. e, Image captured by the compound eye type camera. Inset shows the original object. f, Experimental setup of the compound eye type camera to see two different objects. g, Images acquired by the compound eye type camera of two objects located at different distances. Reproduced with permission [124]. Copyright 2013, Nature Publishing Group.

be well focused on the h-SiNR-PDA after refraction through the lens (Fig. 9c). Fig. 9d demonstrated a 23 × 23 h-SiNR-PDA with an open mesh structure and its individual pixel. Each pixel consists of a Si nanorod photodiode and a blocking diode connected in an n-p-n junction configuration. And the serpentine metal traces were adopted to connect every pixel without mechanical and electrical failures. A thin layer of Al_2O_3 film was deposited on the Si nanorod to suppress the leakage current and reduce charge carrier recombination through passive dangling bonds on the nanorod surface [120–122]. After Al_2O_3 passivation, the photosensitivity of the Si photodiode was obviously enhanced (Fig. 9e). Fig. 9f showed the I-V characteristic of a Si photodiode connected with a blocking diode in series under different light intensities, confirming the suppressing of the reverse current by the blocking diode. These asymmetric I-V curves minimized the crosstalk between neighboring pixels. To validate the imaging features of the aquatic vision-inspired imaging system, the objects were positioned at various distances and angles while the lens was fixed and the position of h-SiNR-PDA was tunable. Fig. 9g demonstrated the imaging result of the device. The captured fish-shaped image was rendered on a hemispherical surface which well match its original shape (inset in Fig. 9g), confirming the function of wide FoV imaging without optical aberration. This device also possessed the features of deep DoF. As shown in Fig. 9h, the device can simultaneously capture two objects, including a triangle and a square, placed at different distances and angles. A blurry image can be refocused on the curved device by tuning the distance between the lens and device, which was the visual accommodation process (Fig. 9i).

4.3. Compound eye-inspired curved imaging system

The compound eyes, found in arthropods and composed of many ommatidia, feature an exceptionally wide FoV, infinite DoF, and high sensitivity to motion [123]. Each ommatidium possesses its own lens and photoreceptor, oriented on a hemispherical surface slightly

differently. Song et al. presented a complete apposition digital camera that are mimic the hemispherical compound eyes [124]. As shown in Fig. 10a, the camera consisted of an array of convex microlenses that provide the optical functions and define the mechanical shape. A hemispherical photodetector array enables the light detection and electrical signal readout. Fig. 10b demonstrated an optical image of the system deformed to a full hemispherical shape. The photodetector array adopted the open mesh configuration to ensure mechanical robustness, where the serpentine Au traces connected the individual pixel composed of a Si photodiode and a blocking diode. Mimicking the ommatidia of the compound eye, each pixel of the photodetector array was placed at the focal position of a corresponding microlens without misalignment under mechanical deformation (Fig. 10c). Fig. 10d showed the conceptual view of the image formation of the compound eye type camera with an 8 × 8 hemispherical photodetector array. A "+" shaped object was projected on the camera and each microlens generated an image with a form decided by the viewing angle and lens parameters. Only the pixels that were overlapped with the projected image by the corresponding lens can generate the proportional photocurrent. Thus, a rough image of the object was captured. To further improve the image resolution, the camera scanned the object mimicking the rapid motion of the eye in biology. The image of a fly line-art pattern was successfully captured by the camera, which was rendered on a hemispherical surface with similar dimensions to the camera (Fig. 10e). Due to the short focal length of the microlens and the image formation mechanism, this camera possessed the property of nearly infinite DoF. As shown in Fig. 10f, two objects with different shapes were placed with the same symmetrical angle of 40° but at different distances. As the circular object moved array from the camera, the image became small but remained in focus, while the image of the triangle object was almost unchanged (Fig. 10f). This confirmed that the compound eye-type camera could simultaneously capture multiple objects with various distances and angles in an aberration-free manner.

5. Human visual perception system-inspired curved neuromorphic imaging system

Artificial visual perception system, combing the imaging, storing, and processing technologies, has enabled diverse image-based tasks with efficient acquisition and recognition, such as moving object detection, facial recognition [125–128]. Currently, conventional imaging systems are widely used for image recognition [129,130]. As shown in Fig. 11a, the image recognition task starts from massive optical signal acquisition based on the flat image sensor with multiple lenses and is followed by the data storage in a memory device. Then, the raw data is processed by the central processing unit (CPU) through iteratively transferring between the CPU and a memory device. A post-processor completes the feature extraction and recognition, including the graphic processing unit (GPU) or neuromorphic chip [131]. Utilizing the multiple optic lenses and iterative data transferring between CPU and memory unit enhanced the system complexity with high power consumption and low efficiency [132,133].

In the human visual system, objects are imaged by the hemispherical retina through a single lens, and then transferred to the visual cortex and recognized by the neural network [114]. In addition, the sensory neurons in the retina can also perform the image pre-processing before the final signal processing in the visual cortex. Mimicking the image processing manner of the human visual system, the neuromorphic imaging system has been proposed with imaging and pre-processing capabilities (Fig. 11b and c). The neuromorphic sensor could convert the optical input into a weighted electrical signal, derive the pre-processed image from massive optical information, and transfer it to the post-processor for image recognition [134–136]. Compared with the flat neuromorphic sensor, the curved device requires a simple optics design and captures images without aberration, which can effectively improve the efficiency of data post-processing. Choi et al. demonstrated a curved neuromorphic imaging system that combined a curved image sensor and a plano-convex lens with housing to support these two elements (Fig. 12a) [131]. As shown in Fig. 12b, the heterostructure of MoS_2 and poly(1,3,5-trimethyl-1,3,5-trivinyl cyclotrisiloxane) (pV3D3) was adopted due to its high responsivity and intrinsic flexibility, and fragile Si_3N_4 film was placed underneath of the phototransistor for strain-releasing design. Employing the ultrathin device structure further minimized the strain in the deformed device to be less than 0.053%. Combining the structure design and material property, the device can be deformed and laminated on a concave hemispherical surface without electrical and mechanical failures (Fig. 12c). The function of image pre-processing was implemented by the integrated imaging system, as shown in Fig. 12d-g. A noisy "C"-shaped optical stimuli consisting of frequent 20 optical spikes was applied on the system (panel (i) in Fig. 12d), while a designated pixel was illuminated by an infrequent spike (panel (i) in Fig. 12g). Consequently, a large photocurrent was accumulated in the pixels under frequent light stimulation while the pixel under the infrequent spike generated a negligible photocurrent, resulting in a pre-processed "C"-shaped image, as shown in the panel (i) in Fig. 12d-g. The acquired image could be maintained for 30 s and entirely erased by a positive gate voltage pulse (panel (ii) and (iii) in Fig. 12d-g). Then, another imaging process of the "N" shaped image

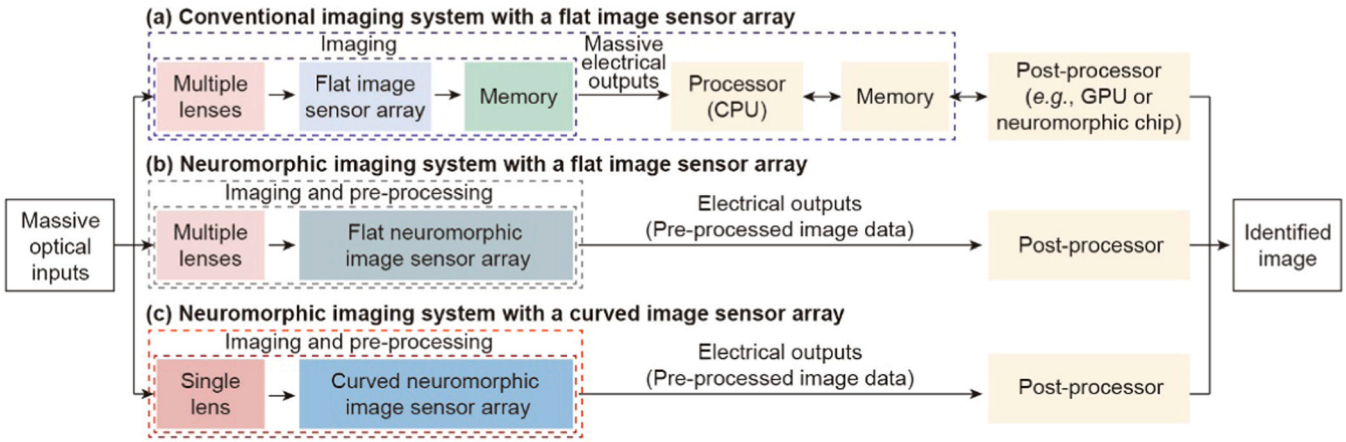

Fig. 11. Blocking diagram showing the process of image recognition by using (a) conventional imaging system with a flat image sensor and neuromorphic imaging system with the (b) flat and (c) curved image sensors. Reproduced with permission [131]. Copyright 2020, Nature Publishing Group.

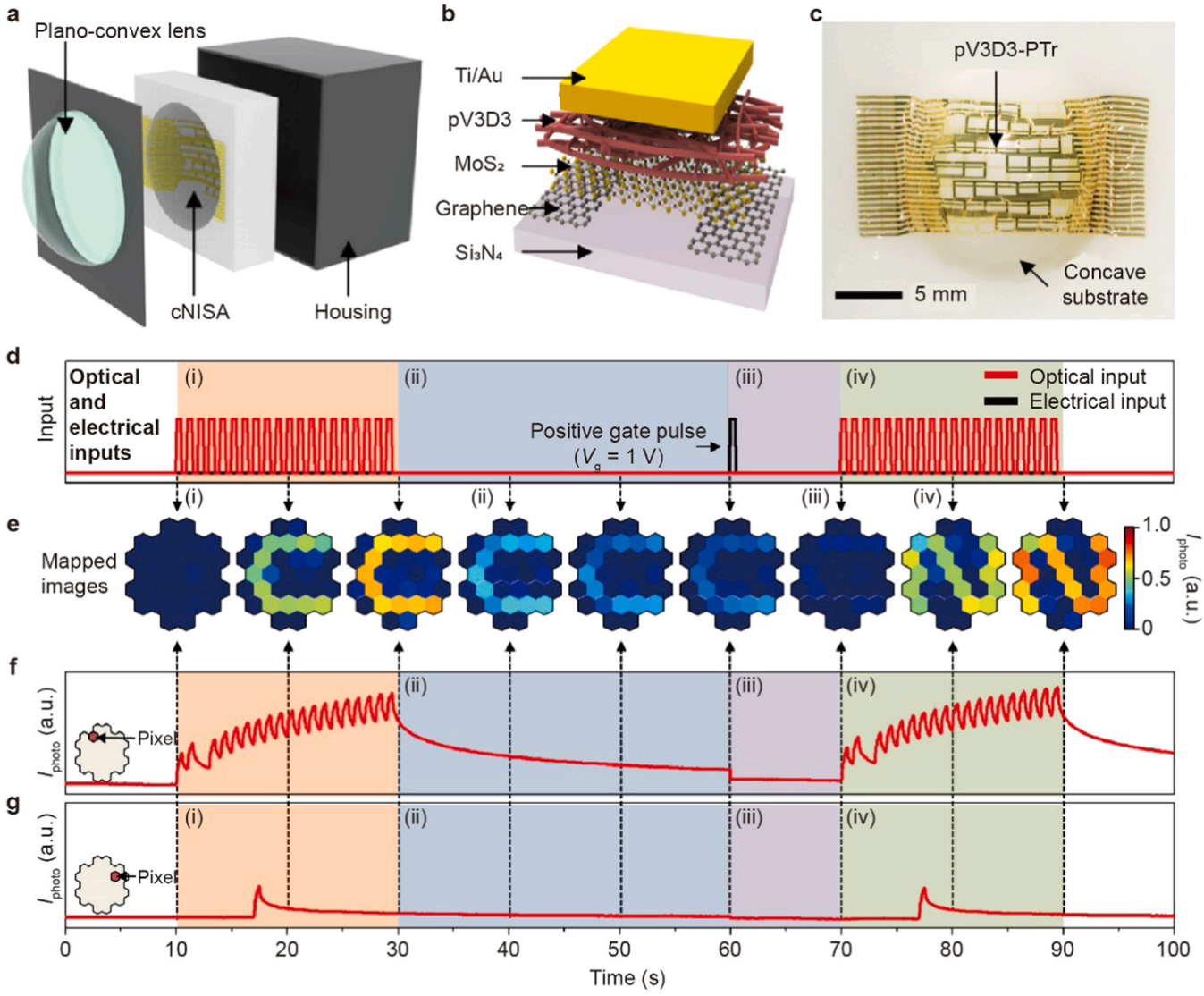

Fig. 12. Human visual recognition system inspired curved neuromorphic imaging sensor. a, Schematic illustration of the curved neuromorphic imaging device. b, Device structure of the MoS_2-pV3D3 phototransistor. c, Optical image of the neuromorphic MoS_2-pV3D3 phototransistor array laminated on a concave substrate. d, Optical and electrical inputs applied on the curved neuromorphic imaging device. e, Image obtained by the curved neuromorphic imaging device under external stimuli from (d). f-g, Photocurrent of the pointed pixel under the external stimuli from (d). Reproduced with permission [131]. Copyright 2020, Nature Publishing Group.

was performed (panel (iv) in Fig. 12d-g), confirming the capability of neuromorphic acquisition of the pre-processing image from the massive noisy optical signals.

6. Summary and perspectives

In nature, most of the visual systems possess a curved retina, which offers unprecedented features of wide FoV, deep DoF, and low optical aberration with only one lens. Inspired by its structure, curved image sensors have been widely studied and integrated with optics as the curved imaging system, which are considered as the next major innovation for the imaging industry. Here, we reviewed the state-of-the-art curved image sensor with advanced fabrication strategies for 3D hemispherical architectures as well as their applications in various biomimetic curved imaging systems.

Currently, the major challenge of the curved image sensor is to fabricate highly curved devices with superior array resolution. Novel strategies have been proposed for curved devices. The most investigated method is to fabricate device on a planar surface followed by either transfer printing or folding to deform the devices into a curved shape. For instance, utilizing the kirigami/origami design enables directly and continuously 2D to 3D transformation via folding, bending, or twisting the structures. Transfer printing of the planar device with open mesh structure onto the rubber substrate offers it excellent stretchability for lamination on the non-developable surface. And employing the ultrathin structure or curved template directly integrates the device with a hemispherically shaped surface. In addition, various semiconductor materials have been explored for the curved device to extend the functions. Si p-i-n junction-based photodiode and blocking diode have been adopted for crosstalk-free imaging in the NIR region. Intrinsically flexible 2D materials, such as MoS_2, graphene, and organic semiconductor improved the mechanical robustness with high responsivity. While successful in concept, these strategies demonstrated low pixel density and large pixel dimension limited by the device stretching and folding. The ideal curved image sensor should possess the comparable imaging performance of commercially-available state-of-art imager, but also the tunable curvature which is particular to the specific optical requirements. Currently, a commercially-available Si-based CMOS image sensor could be curved by the specialized shaping techniques; however, only minor curvature was successfully introduced [137]. Thus, innovation in the manufacturing techniques

for high pixel density device is required, which also should be compatible with various types of imaging sensors, including CCD, CMOS, and front side or back side illuminated sensors. Additionally, the trade-off among device curvature, FoV and volume of the imaging system is still challenging for high quality image acquisition. Generally, the highly curved device could provide wide FoV, which also requires large curvature of the optical lens, resulting in the volume increasing of the total system. Open mesh structure, which is widely investigated, offers tunable device curvature with excellent mechanical robustness, however, the serpentine traces require large space and lead to a small pixel density. The truncated icosahedron structure with a delicate interconnect design could be a promising approach to minimize the device volume and improve the pixel density. Finally, the imaging performance of the curved image sensor should be greatly enhanced. The curved image sensor can implement the basic function of the biological eyes. However, compared with the traditional cameras, either the novel function or the image quality, such as the macrophotography, zoom short, should be developed. Overall, the curved image sensor overcomes the hardware limit of the traditional planar device and has been successfully demonstrated in concept, which will inspire the innovation of imaging system design, manufacturing procedures, etc. to lead to marvelous bionic cameras, thereby providing applications in the smartphone, aerospace, and drones.

CRediT authorship contribution statement

Wenchao Gao: Conceptualization, Investigation, Writing – original draft. **Zhangsheng Xu:** Writing – original draft. **Xun Han:** Conceptualization, Investigation, Writing – original draft, Writing – review & editing. **Caofeng Pan:** Conceptualization, Investigation, Writing – original draft, Writing – review & editing, Funding acquisition.

Declaration of Competing Interest

The authors declare that they have no known competing financial interests or personal relationships that could have appeared to influence the work reported in this paper.

Acknowledgements

The authors thank the support of National Natural Science Foundation of China (No. 52125205, U20A20166, 61675027, 61805015 and 61804011), Natural Science Foundation of Beijing Municipality (Z180011), Shenzhen Science and Technology Program (Grant No. KQTD20170810105439418), GuangDong Basic and Applied Basic Research Foundation (2020A1515110740) and the Fundamental Research Funds for the Central Universities.

References

[1] M. Friedrich, Ancient mechanisms of visual sense organ development based on comparison of the gene networks controlling larval eye, ocellus, and compound eye specification in Drosophila, Arthropod Struct. Dev. 35 (2006) 357.
[2] A.M. Mass, A.Y. Supin, Adaptive features of aquatic mammals' eye, Anat. Rec. 290 (2007) 701.
[3] J.B. Jonas, U. Schneider, G.O. Naumann, Count and density of human retinal photoreceptors, Graefes Arch. Clin. Exp. Ophthalmol. 230 (1992) 505.
[4] P. Artal, Optics of the eye and its impact in vision: a tutorial, Adv. Opt. Photonics 6 (2014) 340.
[5] H.-J. Wagner, E. Fröhlich, K. Negishi, S. Collin, The eyes of deep-sea fish II. Functional morphology of the retina, Prog. Retin. Eye Res. 17 (1998) 637.
[6] L. Chittka, Bee color vision is optimal for coding flower color, but flower colors are not optimal for being coded—why? Isr. J. Plant Sci. 45 (1997) 115.
[7] D.A. Atchison, G. Smith, G. Smith, Optics of the human eye, Butterworth-Heinemann Oxford, 2000.
[8] J.J. Nassi, E.M. Callaway, Parallel processing strategies of the primate visual system, Nat. Rev. Neurosci. 10 (2009) 360.
[9] W. Jagger, P. Sands, A wide-angle gradient index optical model of the crystalline lens and eye of the rainbow trout, Vis. Res. 36 (1996) 2623.
[10] W.S. Jagger, P. Sands, A wide-angle gradient index optical model of the crystalline lens and eye of the octopus, Vis. Res. 39 (1999) 2841.
[11] K.-H. Jeong, J. Kim, L.P. Lee, Biologically inspired artificial compound eyes, Science 312 (2006) 557.
[12] D. Floreano, R. Pericet-Camara, S. Viollet, F. Ruffier, A. Brückner, R. Leitel, W. Buss, M. Menouni, F. Expert, R. Juston, Miniature curved artificial compound eyes, Proc. Natl. Acad. Sci. U. S. A 110 (2013) 9267.
[13] L.C. Kogos, Y. Li, J. Liu, Y. Li, L. Tian, R. Paiella, Plasmonic ommatidia for lensless compound-eye vision, Nat. Commun. 11 (2020) 1.
[14] S. Wu, T. Jiang, G. Zhang, B. Schoenemann, F. Neri, M. Zhu, C. Bu, J. Han, K.-D. Kuhnert, Artificial compound eye: a survey of the state-of-the-art, Artif. Intell. Rev. 48 (2017) 573.
[15] Y. Zhai, Q. Han, J. Niu, J. Liu, B. Yang, Microfabrication of bioinspired curved artificial compound eyes: a review, Microsyst. Technol. 27 (2021) 3241.
[16] G.J. Lee, C. Choi, D.H. Kim, Y.M. Song, Bioinspired artificial eyes: optic components, digital cameras, and visual prostheses, Adv. Funct. Mater. 28 (2018) 1705202.
[17] J.-U. Lee, S.-M. Yu, Analytic design procedure of three-mirror telescope corrected for spherical aberration, coma, astigmatism, and Petzval field curvature, J. Opt. Soc. Korea 13 (2009) 184.
[18] T. Chung, Y. Lee, S.P. Yang, K. Kim, B.H. Kang, K.H. Jeong, Mining the smartness of insect ultrastructures for advanced imaging and illumination, Adv. Funct. Mater. 28 (2018) 1705912.
[19] R.P. Jonas, M.D. Thorpe, International Optical Design Conference, Optical Society of America, pp. MB2.
[20] G.J. Lee, W.I. Nam, Y.M. Song, Robustness of an artificially tailored fisheye imaging system with a curvilinear image surface, Opt. Laser Technol. 96 (2017) 50.
[21] H. Liu, Y. Huang, H. Jiang, Artificial eye for scotopic vision with bioinspired all-optical photosensitivity enhancer, Proc. Natl. Acad. Sci. U. S. A 113 (2016) 3982.
[22] S.-B. Rim, P.B. Catrysse, R. Dinyari, K. Huang, P. Peumans, The optical advantages of curved focal plane arrays, Opt. Express 16 (2008) 4965.
[23] C. Pan, J. Zhai, Z.L. Wang, Piezotronics and piezo-phototronics of third generation semiconductor nanowires, Chem. Rev. 119 (2019) 9303.
[24] Y. Peng, J. Lu, D. Peng, W. Ma, F. Li, Q. Chen, X. Wang, J. Sun, H. Liu, C. Pan, Dynamically modulated GaN whispering gallery lasing mode for strain sensor, Adv. Funct. Mater. 29 (2019) 1905051.
[25] K. Zhou, Y. Zhao, X. Sun, Z. Yuan, G. Zheng, K. Dai, L. Mi, C. Pan, C. Liu, C. Shen, Ultra-stretchable triboelectric nanogenerator as high-sensitive and self-powered electronic skins for energy harvesting and tactile sensing, Nano Energy 70 (2020) 104546.
[26] C. Pan, L. Dong, G. Zhu, S. Niu, R. Yu, Q. Yang, Y. Liu, Z.L. Wang, High-resolution electroluminescent imaging of pressure distribution using a piezoelectric nanowire LED array, Nat. Photon. 7 (2013) 752.
[27] J. Sun, Q. Hua, R. Zhou, D. Li, W. Guo, X. Li, G. Hu, C. Shan, Q. Meng, L. Dong, Piezo-phototronic effect enhanced efficient flexible perovskite solar cells, ACS Nano 13 (2019) 4507.
[28] M. Que, W. Guo, X. Zhang, X. Li, Q. Hua, L. Dong, C. Pan, Flexible quantum dot-sensitized solar cells employing CoS nanorod arrays/graphite paper as effective counter electrodes, J. Mater. Chem. A 2 (2014) 13661.
[29] C. Wang, J. Zhao, C. Ma, J. Sun, L. Tian, X. Li, F. Li, X. Han, C. Liu, C. Shen, Detection of non-joint areas tiny strain and anti-interference voice recognition by micro-cracked metal thin film, Nano Energy 34 (2017) 578.
[30] H. Ren, N. Cui, Q. Tang, Y. Tong, X. Zhao, Y. Liu, High-performance, ultrathin, ultraflexible organic thin-film transistor array via solution process, Small 14 (2018) 1801020.
[31] C. Wang, C. Pan, Z. Wang, Electronic skin for closed-loop systems, ACS Nano 13 (2019) 12287.
[32] K. Xia, W. Wu, M. Zhu, X. Shen, Z. Yin, H. Wang, S. Li, M. Zhang, H. Wang, H. Lu, CVD growth of perovskite/graphene films for high-performance flexible image sensor, Sci. Bull. 65 (2020) 343.
[33] H. Liu, X. Chen, Y. Zheng, D. Zhang, Y. Zhao, C. Wang, C. Pan, C. Liu, C. Shen, Lightweight, superelastic, and hydrophobic polyimide nanofiber/MXene composite aerogel for wearable piezoresistive sensor and oil/water separation applications, Adv. Funct. Mater. 31 (2021) 2008006.
[34] K. Zhou, W. Xu, Y. Yu, W. Zhai, Z. Yuan, K. Dai, G. Zheng, L. Mi, C. Pan, C. Liu, Tunable and Nacre-mimetic multifunctional electronic skins for highly stretchable contact-noncontact sensing, Small 17 (2021) 2100542.
[35] J. Sun, Y. Chang, L. Dong, K. Zhang, Q. Hua, J. Zang, Q. Chen, Y. Shang, C. Pan, C. Shan, MXene enhanced self-powered alternating current electroluminescence devices for patterned flexible displays, Nano Energy 86 (2021) 106077.
[36] S.-K. Su, C.-P. Chuu, M.-Y. Li, C.-C. Cheng, H.S.P. Wong, L.-J. Li, Layered semiconducting 2D materials for future transistor applications, Small Struct. 2 (2021) 2000103.
[37] S. Sinha, J.H. Warner, Recent progress in using graphene as an ultrathin transparent support for transmission electron microscopy, Small Struct. 2 (2021) 2000049.
[38] J. Wu, H. Ma, P. Yin, Y. Ge, Y. Zhang, L. Li, H. Zhang, H. Lin, Two-dimensional materials for integrated photonics: recent advances and future challenges, Small Sci. 1 (2021) 2000053.
[39] J. Zang, F. Liu, Modified timoshenko formula for bending of ultrathin strained bilayer films, Appl. Phys. Lett. 92 (2008) 021905.

[40] W. Wu, X. Han, J. Li, X. Wang, Y. Zhang, Z. Huo, Q. Chen, X. Sun, Z. Xu, Y. Tan, C. Pan, A. Pan, Ultrathin and conformable lead halide perovskite photodetector arrays for potential application in retina-like vision sensing, Adv. Mater. 33 (2021) 2006006.
[41] K.Y. Thai, I. Park, B.J. Kim, A.T. Hoang, Y. Na, C.U. Park, Y. Chae, J.-H. Ahn, MoS2/graphene photodetector array with strain-modulated photoresponse up to the near-infrared regime, ACS Nano 15 (2021) 12836.
[42] R. Bao, C. Wang, Z. Peng, C. Ma, L. Dong, C. Pan, Light-emission enhancement in a flexible and size-controllable ZnO nanowire/organic light-emitting diode array by the piezotronic effect, ACS Photonics 4 (2017) 1344.
[43] C. Wang, D. Peng, J. Zhao, R. Bao, T. Li, L. Tian, L. Dong, C. Shen, C. Pan, CdS@ SiO2 core–shell electroluminescent nanorod arrays based on a metal–insulator–semiconductor structure, Small 12 (2016) 5734.
[44] X. Wang, H. Zhang, R. Yu, L. Dong, D. Peng, A. Zhang, Y. Zhang, H. Liu, C. Pan, Z.L. Wang, Dynamic pressure mapping of personalized handwriting by a flexible sensor matrix based on the mechanoluminescence process, Adv. Mater. 27 (2015) 2324.
[45] R. Bao, C. Wang, L. Dong, R. Yu, K. Zhao, Z.L. Wang, C. Pan, Flexible and controllable piezo-phototronic pressure mapping sensor matrix by ZnO NW/p-polymer LED array, Adv. Funct. Mater. 25 (2015) 2884.
[46] R. Yu, L. Dong, C. Pan, S. Niu, H. Liu, W. Liu, S. Chua, D. Chi, Z.L. Wang, Piezotronic effect on the transport properties of GaN nanobelts for active flexible electronics, Adv. Mater. 24 (2012) 3532.
[47] C. Pan, W. Guo, L. Dong, G. Zhu, Z.L. Wang, Optical fiber-based core–shell coaxially structured hybrid cells for self-powered nanosystems, Adv. Mater. 24 (2012) 3356.
[48] R. Bao, C. Wang, L. Dong, C. Shen, K. Zhao, C. Pan, CdS nanorods/organic hybrid LED array and the piezo-phototronic effect of the device for pressure mapping, Nanoscale 8 (2016) 8078.
[49] R. Xiang, S. Maruyama, Heteronanotubes: challenges and opportunities, Small Sci. 1 (2021) 2000039.
[50] W. Wu, X. Wang, X. Han, Z. Yang, G. Gao, Y. Zhang, J. Hu, Y. Tan, A. Pan, C. Pan, Flexible photodetector arrays based on patterned CH3NH3PbI3− xClx perovskite film for real-time photosensing and imaging, Adv. Mater. 31 (2019) 1805913.
[51] F. Li, J. Lu, Q. Zhang, D. Peng, Z. Yang, Q. Xu, C. Pan, A. Pan, T. Li, R. Wang, Controlled fabrication, lasing behavior and excitonic recombination dynamics in single crystal CH3NH3PbBr3 perovskite cuboids, Sci. Bull. 64 (2019) 698.
[52] D. Peng, X. Liu, C. Pan, Epitaxial lift-off for controllable single-crystalline perovskites, Sci. Bull. 66 (2021) 6.
[53] F. Li, Z. Xia, C. Pan, Y. Gong, L. Gu, Q. Liu, J.Z. Zhang, High Br–content CsPb (Cl y Br1–y) 3 perovskite nanocrystals with strong Mn2+ emission through diverse cation/anion exchange engineering, Acs Appl. Mater. Inter. 10 (2018) 11739.
[54] X. Han, W. Wu, H. Chen, D. Peng, L. Qiu, P. Yan, C. Pan, Metal halide perovskite arrays: from construction to optoelectronic applications, Adv. Funct. Mater. 31 (2021) 2005230.
[55] J. Sun, N. Li, L. Dong, X. Niu, M. Zhao, Z. Xu, H. Zhou, C. Shan, C. Pan, Interfacial-engineering enhanced performance and stability of ZnO nanowire-based perovskite solar cells, Nanotechnology 32 (2021) 475204.
[56] J. Sun, Q. Hua, M. Zhao, L. Dong, Y. Chang, W. Wu, J. Li, Q. Chen, J. Xi, W. Hu, Stable ultrathin perovskite/polyvinylidene fluoride composite films for imperceptible multi-color fluorescent anti-counterfeiting labels, Adv. Mater. Technol. (2021) 2100229.
[57] Y. Sun, T. Liu, Y. Kan, K. Gao, B. Tang, Y. Li, Flexible organic solar cells: progress and challenges, Small Sci. 1 (2021) 2100001.
[58] K. Zhang, Y.H. Jung, S. Mikael, J.-H. Seo, M. Kim, H. Mi, H. Zhou, Z. Xia, W. Zhou, S. Gong, Z. Ma, Origami silicon optoelectronics for hemispherical electronic eye systems, Nat. Commun. 8 (2017) 1.
[59] S. Chen, J. Chen, X. Zhang, Z.-Y. Li, J. Li, Kirigami/origami: unfolding the new regime of advanced 3D microfabrication/nanofabrication with “folding”, Light Sci. Appl. 9 (2020) 1.
[60] S.A. Zirbel, R.J. Lang, M.W. Thomson, D.A. Sigel, P.E. Walkemeyer, B.P. Trease, S.P. Magleby, L.L. Howell, Accommodating thickness in origami-based deployable arrays, J. Mech. Des. 135 (2013).
[61] J. Rogers, Y. Huang, O.G. Schmidt, D.H. Gracias, Origami mems and nems, MRS Bull. 41 (2016) 123.
[62] J.S. Randhawa, T.G. Leong, N. Bassik, B.R. Benson, M.T. Jochmans, D.H. Gracias, Pick-and-place using chemically actuated microgrippers, J. Am. Chem. Soc. 130 (2008) 17238.
[63] S. Pandey, M. Ewing, A. Kunas, N. Nguyen, D.H. Gracias, G. Menon, Algorithmic design of self-folding polyhedra, Proc. Natl. Acad. Sci. U. S. A 108 (2011) 19885.
[64] H. Chen, X.-L. Zhang, Y.-Y. Zhang, D. Wang, D.-L. Bao, Y. Que, W. Xiao, S. Du, M. Ouyang, S.T. Pantelides, Atomically precise, custom-design origami graphene nanostructures, Science 365 (2019) 1036.
[65] J.L. Silverberg, A.A. Evans, L. McLeod, R.C. Hayward, T. Hull, C.D. Santangelo, I. Cohen, Using origami design principles to fold reprogrammable mechanical metamaterials, Science 345 (2014) 647.
[66] Z. Wang, L. Jing, K. Yao, Y. Yang, B. Zheng, C.M. Soukoulis, H. Chen, Y. Liu, Origami-based reconfigurable metamaterials for tunable chirality, Adv. Mater. 29 (2017) 1700412.
[67] Z. Liu, H. Du, J. Li, L. Lu, Z.-Y. Li, N.X. Fang, Nano-kirigami with giant optical chirality, Sci. Adv. 4 (2018) eaat4436.
[68] W. Lee, Y. Liu, Y. Lee, B.K. Sharma, S.M. Shinde, S.D. Kim, K. Nan, Z. Yan, M. Han, Y. Huang, Y. Zhang, J.-H. Ahn, J. Rogers, Two-dimensional materials in functional three-dimensional architectures with applications in photodetection and imaging, Nat. Commun. 9 (2018) 1.
[69] Y. Chen, Y. Lu, M. Liao, Y. Tian, Q. Liu, C. Gao, X. Yang, C. Shan, 3D solar-blind Ga2O3 photodetector array realized via origami method, Adv. Funct. Mater. 29 (2019) 1906040.
[70] R. Grantab, V.B. Shenoy, R.S. Ruoff, Anomalous strength characteristics of tilt grain boundaries in graphene, Science 330 (2010) 946.
[71] S.-K. Lee, B.J. Kim, H. Jang, S.C. Yoon, C. Lee, B.H. Hong, J.A. Rogers, J.H. Cho, J.-H. Ahn, Stretchable graphene transistors with printed dielectrics and gate electrodes, Nano Lett. 11 (2011) 4642.
[72] P. Zhang, L. Ma, F. Fan, Z. Zeng, C. Peng, P.E. Loya, Z. Liu, Y. Gong, J. Zhang, X. Zhang, Fracture toughness of graphene, Nat. Commun. 5 (2014) 1.
[73] J. Tan, S. Li, B. Liu, H.-M. Cheng, Structure, preparation, and applications of 2D material-based metal–semiconductor heterostructures, Small Struct. 2 (2021) 2000093.
[74] J. Li, Z. Liu, Focused-ion-beam-based nano-kirigami: from art to photonics, Nanophotonics 7 (2018) 1637.
[75] B.F. Grosso, E.J. Mele, Bending rules in graphene kirigami, Phys. Rev. Lett. 115 (2015) 195501.
[76] T. Castle, Y. Cho, X. Gong, E. Jung, D.M. Sussman, S. Yang, R.D. Kamien, Making the cut: lattice kirigami rules, Phys. Rev. Lett. 113 (2014) 245502.
[77] X. Han, K.J. Seo, Y. Qiang, Z. Li, S. Vinnikova, Y. Zhong, X. Zhao, P. Hao, S. Wang, H. Fang, Nanomeshed Si nanomembranes, npj Flex, Electron 3 (2019) 1.
[78] M.K. Blees, A.W. Barnard, P.A. Rose, S.P. Roberts, K.L. McGill, P.Y. Huang, A.R. Ruyack, J.W. Kevek, B. Kobrin, D.A. Muller, Graphene kirigami, Nature 524 (2015) 204.
[79] Z. Rao, Y. Lu, Z. Li, K. Sim, Z. Ma, J. Xiao, C. Yu, Curvy, shape-adaptive imagers based on printed optoelectronic pixels with a kirigami design, Nat. Electron. (2021) 1.
[80] D.H. Kim, J.A. Rogers, Stretchable electronics: materials strategies and devices, Adv. Mater. 20 (2008) 4887.
[81] T. Wu, S.S. Hamann, A.C. Ceballos, C.-E. Chang, O. Solgaard, R.T. Howe, Design and fabrication of silicon-tessellated structures for monocentric imagers, Microsyst. Nanoeng. 2 (2016) 1.
[82] C. Choi, M.K. Choi, S. Liu, M.S. Kim, O.K. Park, C. Im, J. Kim, X. Qin, G.J. Lee, K.W. Cho, M. Kim, E. Joh, J. Lee, D. Son, S.-H. Kwon, N.L. Jeon, Y.M. Song, N. Lu, D.-H. Kim, Human eye-inspired soft optoelectronic device using high-density MoS 2-graphene curved image sensor array, Nat. Commun. 8 (2017) 1.
[83] Z. Komeily-Nia, L.-T. Qu, J.-L. Li, Progress in the understanding and applications of the intrinsic reactivity of graphene-based materials, Small Sci. 1 (2021) 2000026.
[84] Y. Gong, X. Xing, Y. Wang, Z. Lv, Y. Zhou, S.-T. Han, Emerging MXenes for functional memories, Small Sci. 1 (2021) 2100006.
[85] G. Yun, S.-Y. Tang, H. Lu, S. Zhang, M.D. Dickey, W. Li, Hybrid-filler stretchable conductive composites: from fabrication to application, Small Sci. (2021) 2000080.
[86] R. Bao, J. Tao, C. Pan, Z.L. Wang, Piezophototronic effect in nanosensors, Small Sci. (2021) 2000060.
[87] J. Ren, P. Innocenzi, 2D boron nitride heterostructures: recent advances and future challenges, Small Struct. (2021) 2100068.
[88] S.I. Park, J.H. Ahn, X. Feng, S. Wang, Y. Huang, J.A. Rogers, Theoretical and experimental studies of bending of inorganic electronic materials on plastic substrates, Adv. Funct. Mater. 18 (2008) 2673.
[89] Y. Zhang, Z. Yan, K. Nan, D. Xiao, Y. Liu, H. Luan, H. Fu, X. Wang, Q. Yang, J. Wang, A mechanically driven form of Kirigami as a route to 3D mesostructures in micro/nanomembranes, Proc. Natl. Acad. Sci. U. S. A 112 (2015) 11757.
[90] W. Liu, Q. Zou, C. Zheng, C. Jin, Metal-assisted transfer strategy for construction of 2D and 3D nanostructures on an elastic substrate, ACS Nano 13 (2018) 440.
[91] H. Zhao, K. Li, M. Han, F. Zhu, A. Vázquez-Guardado, P. Guo, Z. Xie, Y. Park, L. Chen, X. Wang, Buckling and twisting of advanced materials into morphable 3D mesostructures, Proc. Natl. Acad. Sci. U. S. A 116 (2019) 13239.
[92] S. Xu, Y. Zhang, J. Cho, J. Lee, X. Huang, L. Jia, J.A. Fan, Y. Su, J. Su, H. Zhang, Stretchable batteries with self-similar serpentine interconnects and integrated wireless recharging systems, Nat. Commun. 4 (2013) 1.
[93] H.C. Ko, M.P. Stoykovich, J. Song, V. Malyarchuk, W.M. Choi, C.-J. Yu, J.B. Geddes Iii, J. Xiao, S. Wang, Y. Huang, J. Rogers, A hemispherical electronic eye camera based on compressible silicon optoelectronics, Nature 454 (2008) 748.
[94] Q. Hua, J. Sun, H. Liu, R. Bao, R. Yu, J. Zhai, C. Pan, Z.L. Wang, Skin-inspired highly stretchable and conformable matrix networks for multifunctional sensing, Nat. Commun. 9 (2018) 1.
[95] R. Li, M. Li, Y. Su, J. Song, X. Ni, An analytical mechanics model for the island-bridge structure of stretchable electronics, Soft Matter 9 (2013) 8476.
[96] C.A. Silva, J. Lv, L. Yin, I. Jeerapan, G. Innocenzi, F. Soto, Y.G. Ha, J. Wang, Liquid metal based island-bridge architectures for all printed stretchable electrochemical devices, Adv. Funct. Mater. 30 (2020) 2002041.
[97] I. Jung, J. Xiao, V. Malyarchuk, C. Lu, M. Li, Z. Liu, J. Yoon, Y. Huang, J.A. Rogers, Dynamically tunable hemispherical electronic eye camera system with adjustable zoom capability, Proc. Natl. Acad. Sci. U. S. A 108 (2011) 1788.
[98] D. Fan, B. Lee, C. Coburn, S.R. Forrest, From 2D to 3D: strain-and elongation-free topological transformations of optoelectronic circuits, Proc. Natl. Acad. Sci. U. S. A 116 (2019) 3968.
[99] I. Su, Z. Qin, T. Saraceno, A. Krell, R. Mühlethaler, A. Bisshop, M.J. Buehler, Imaging and analysis of a three-dimensional spider web architecture, J. R. Soc. Interface 15 (2018) 20180193.
[100] H.R. Namazi, The complexity based analysis of the correlation between spider's brain signal and web, ARC J. Neurosci. 2 (2017) 38.

[101] Q. He, J. Feng, Y. Chen, H. Zhou, Mechanical properties of spider-web hierarchical honeycombs subjected to out-of-plane impact loading, J. Sandw. Struct. Mater. 22 (2020) 771.
[102] Y. Aoyanagi, K. Okumura, Simple model for the mechanics of spider webs, Phys. Rev. Lett. 104 (2010) 038102.
[103] S.W. Cranford, A. Tarakanova, N.M. Pugno, M.J. Buehler, Nonlinear material behaviour of spider silk yields robust webs, Nature 482 (2012) 72.
[104] X. Liu, D. Liu, J.-h Lee, Q. Zheng, X. Du, X. Zhang, H. Xu, Z. Wang, Y. Wu, X. Shen, Spider-web-inspired stretchable graphene woven fabric for highly sensitive, transparent, wearable strain sensors, Acs Appl. Mater. Inter. 11 (2018) 2282.
[105] E.K. Lee, R.K. Baruah, J.W. Leem, W. Park, B.H. Kim, A. Urbas, Z. Ku, Y.L. Kim, M.A. Alam, C.H. Lee, Fractal web design of a hemispherical photodetector array with organic-dye-sensitized graphene hybrid composites, Adv. Mater. 32 (2020) 2004456.
[106] M.A. Meitl, Z.-T. Zhu, V. Kumar, K.J. Lee, X. Feng, Y.Y. Huang, I. Adesida, R.G. Nuzzo, J.A. Rogers, Transfer printing by kinetic control of adhesion to an elastomeric stamp, Nat. Mater. 5 (2006) 33.
[107] A. Carlson, A.M. Bowen, Y. Huang, R.G. Nuzzo, J.A. Rogers, Transfer printing techniques for materials assembly and micro/nanodevice fabrication, Adv. Mater. 24 (2012) 5284.
[108] T.-H. Kim, K.-S. Cho, E.K. Lee, S.J. Lee, J. Chae, J.W. Kim, D.H. Kim, J.-Y. Kwon, G. Amaratunga, S.Y. Lee, Full-colour quantum dot displays fabricated by transfer printing, Nat. Photon. 5 (2011) 176.
[109] L. Gu, S. Poddar, Y. Lin, Z. Long, D. Zhang, Q. Zhang, L. Shu, X. Qiu, M. Kam, A. Javey, Z. Fan, A biomimetic eye with a hemispherical perovskite nanowire array retina, Nature 581 (2020) 278.
[110] G. Boschloo, A. Hagfeldt, Characteristics of the iodide/triiodide redox mediator in dye-sensitized solar cells, Acc. Chem. Res. 42 (2009) 1819.
[111] H.K. Raut, V.A. Ganesh, A.S. Nair, S. Ramakrishna, Anti-reflective coatings: a critical, in-depth review, Energy Environ. Sci. 4 (2011) 3779.
[112] E. Lurie-Luke, Product and technology innovation: what can biomimicry inspire? Biotechnol. Adv. 32 (2014) 1494.
[113] Z. Lou, G. Shen, Flexible image sensors with semiconducting nanowires for biomimic visual applications, Small Struct. 2 (2021) 2000152.
[114] X. Han, Z. Xu, W. Wu, X. Liu, P. Yan, C. Pan, Recent progress in optoelectronic synapses for artificial visual-perception system, Small Struct. 1 (2020) 2000029.
[115] J.F. Koretz, C.A. Cook, P.L. Kaufman, Aging of the human lens: changes in lens shape upon accommodation and with accommodative loss, J. Opt. Soc. Am. A 19 (2002) 144.
[116] N. López-Gil, V. Fernández-Sánchez, The change of spherical aberration during accommodation and its effect on the accommodation response, J. Vis. 10 (2010) 12.
[117] L. Li, Q.-H. Wang, W. Jiang, Liquid lens with double tunable surfaces for large power tunability and improved optical performance, J. Opt. 13 (2011) 115503.
[118] M. Ott, Visual accommodation in vertebrates: mechanisms, physiological response and stimuli, J. Comp. Physiol. A 192 (2006) 97.
[119] M.S. Kim, G.J. Lee, C. Choi, M.S. Kim, M. Lee, S. Liu, K.W. Cho, H.M. Kim, H. Cho, M.K. Choi, N. Lu, Y.M. Song, D.-H. Kim, An aquatic-vision-inspired camera based on a monocentric lens and a silicon nanorod photodiode array, Nat. Electron. 3 (2020) 546.
[120] H. Savin, P. Repo, G. Von Gastrow, P. Ortega, E. Calle, M. Garín, R. Alcubilla, Black silicon solar cells with interdigitated back-contacts achieve 22.1% efficiency, Nat. Nanotechnol. 10 (2015) 624.
[121] X. Li, M. Chen, R. Yu, T. Zhang, D. Song, R. Liang, Q. Zhang, S. Cheng, L. Dong, A. Pan, Enhancing light emission of ZnO-nanofilm/Si-micropillar heterostructure arrays by piezo-phototronic effect, Adv. Mater. 27 (2015) 4447.
[122] S. Qiao, R. Cong, J. Liu, B. Liang, G. Fu, W. Yu, K. Ren, S. Wang, C. Pan, A vertically layered MoS 2/Si heterojunction for an ultrahigh and ultrafast photoresponse photodetector, J. Mater. Chem. C. 6 (2018) 3233.
[123] Y. Cheng, J. Cao, Y. Zhang, Q. Hao, Review of state-of-the-art artificial compound eye imaging systems, Bioinspir. Biomim. 14 (2019) 031002.
[124] Y.M. Song, Y. Xie, V. Malyarchuk, J. Xiao, I. Jung, K.-J. Choi, Z. Liu, H. Park, C. Lu, R.-H. Kim, R. Li, K. Crozier, Y. Huang, J. Rogers, Digital cameras with designs inspired by the arthropod eye, Nature 497 (2013) 95.
[125] F. Zhou, Z. Zhou, J. Chen, T.H. Choy, J. Wang, N. Zhang, Z. Lin, S. Yu, J. Kang, H.S.P. Wong, Optoelectronic resistive random access memory for neuromorphic vision sensors, Nat. Nanotechnol. 14 (2019) 776.
[126] P. Yao, H. Wu, B. Gao, S.B. Eryilmaz, X. Huang, W. Zhang, Q. Zhang, N. Deng, L. Shi, H.S.P. Wong, Face classification using electronic synapses, Nat. Commun. 8 (2017) 1.
[127] K. Roy, A. Jaiswal, P. Panda, Towards spike-based machine intelligence with neuromorphic computing, Nature 575 (2019) 607.
[128] J. Kim, S. Song, Y.-H. Kim, S.K. Park, Recent progress of quantum dot-based photonic devices and systems: a comprehensive review of materials, devices, and applications, Small Struct. 2 (2021) 2000024.
[129] K. Yang, J. Joshua Yang, R. Huang, Y. Yang, Nonlinearity in memristors for neuromorphic dynamic systems, Small Sci. (2021) 2100049.
[130] T. Shi, R. Wang, Z. Wu, Y. Sun, J. An, Q. Liu, A review of resistive switching devices: performance improvement, characterization, and applications, Small Struct. 2 (2021) 2000109.
[131] C. Choi, J. Leem, M.S. Kim, A. Taqieddin, C. Cho, K.W. Cho, G.J. Lee, H. Seung, H.J. Bae, Y.M. Song, T. Hyeon, N.R. Aluru, S. Nam, D.-H. Kim, Curved neuromorphic image sensor array using a MoS 2-organic heterostructure inspired by the human visual recognition system, Nat. Commun. 11 (2020) 1.
[132] M.A. Zidan, J.P. Strachan, W.D. Lu, The future of electronics based on memristive systems, Nat. Electron. 1 (2018) 22.
[133] Y. van De Burgt, A. Melianas, S.T. Keene, G. Malliaras, A. Salleo, Organic electronics for neuromorphic computing, Nat. Electron. 1 (2018) 386.
[134] M. Lee, W. Lee, S. Choi, J.W. Jo, J. Kim, S.K. Park, Y.H. Kim, Brain-inspired photonic neuromorphic devices using photodynamic amorphous oxide semiconductors and their persistent photoconductivity, Adv. Mater. 29 (2017) 1700951.
[135] H. Wang, Q. Zhao, Z. Ni, Q. Li, H. Liu, Y. Yang, L. Wang, Y. Ran, Y. Guo, W. Hu, A ferroelectric/electrochemical modulated organic synapse for ultraflexible, artificial visual-perception system, Adv. Mater. 30 (2018) 1803961.
[136] H. Liu, Q. Hua, R. Yu, Y. Yang, T. Zhang, Y. Zhang, C. Pan, A bamboo-like GaN microwire-based piezotronic memristor, Adv. Funct. Mater. 26 (2016) 5307.
[137] B. Guenter, N. Joshi, R. Stoakley, A. Keefe, K. Geary, R. Freeman, J. Hundley, P. Patterson, D. Hammon, G. Herrera, Highly curved image sensors: a practical approach for improved optical performance, Opt. Express 25 (2017) 13010.